



# Validity, reliability and certainty of PERSIANN and TRMM satellite-derived daily precipitation data in arid and semiarid climates

Keyvan Khojand<sup>1</sup> · Mahmood Reza Shaghaghian<sup>2</sup> · Zahra Ghadampour<sup>1</sup> · Touraj Sabzevari<sup>1</sup>

Received: 17 October 2021 / Accepted: 20 April 2022 / Published online: 26 May 2022

© The Author(s) under exclusive licence to Institute of Geophysics, Polish Academy of Sciences & Polish Academy of Sciences 2022

## Abstract

Having doubts about the adequacy of reliability level of satellite-derived precipitation products, along with their application in large number of hydrological models, has led to many studies on evaluating the efficiency of such data. In this study, two new procedures were proposed to compute reliability and certainty degrees of PERSIANN and TRMM 3B42RT data sets, and six traditional indicators were used to evaluate their validation. In addition, the cumulative density function (cdf) of the above-mentioned data sets was compared with the ground-based observations in 23 synoptic stations in Fars, Iran. The Kolmogorov–Smirnov test was performed using the data sets at 5% significance level which led to the result of null hypothesis that was not being rejected, suggesting that the satellite-derived daily precipitation data (SDDPD) and ground-based observations are drawn from the same distribution. Results indicated that TRMM and PERSIANN follow quite similar probability pattern of ground-based observations in arid and semiarid climate, respectively. However, data probability pattern of TRMM cannot be considered similar to ground-based observations in arid region, neither can PERSIANN in semiarid climate. Among common cross-validating attributes, the values of ME and BIAS, in addition to RMSE and MAE, led to the conclusion that in PERSIANN, the rainfall daily rates are almost underestimated while TRMM overestimates the values mainly in semiarid regions. Moreover, the PERSIANN was found to be significantly correlated with IDM (De Martonne aridity Index), and the values of underestimation increased with growth of the index. The reliability values of SDDPD over the study area, for both TRMM and PERSIANN, show the reverse trend with increasing IDM in almost all acceptable error intervals. Along with effects of climate conditions, the reliability degrees of PERSIANN seem quite more consistent at different acceptable error intervals in comparison with the corresponding values of TRMM. In addition to validity and reliability, the error entropy of SDDPD, as an index for uncertainty degree, increases as the IDM rises, which is theoretically corresponds with reliability concept. However, in comparison with PERSIANN, TRMM data set, overall, has higher degree of uncertainty. In addition, to evaluate effect of daily rainfall intensity on the uncertainty degree of SDDPD, the uncertainty degree slightly increases as daily rainfall intensifies to about 15 mm/day. But for higher daily rainfall intensities, on the other hand, the uncertainty degree seems to gradually decline as the daily rainfall increases.

**Keywords** PERSIANN · TRMM 3B42RT · Arid and semiarid climates · Validity · Reliability · Certainty

## Introduction

Hydrologists and water resources managers are usually confronted with problems that require precise, reliable and validated spatiotemporal rainfall data. These data are often used in various spatial and temporal scales for numerous applications, including water budget studies, reservoir operation, and flood forecasting and control (Shaghaghian and Abedini 2013). The background data required for such inputs are often collected via either ground-based measurements (i.e., in situ rain gauges) or air-based instruments (i.e., radar and satellite imagery). For example, as a broadly used

---

Edited by Dr. Senlin Zhu (ASSOCIATE EDITOR) / Dr. Michael Nones (CO-EDITOR-IN-CHIEF).

✉ Mahmood Reza Shaghaghian  
shaghaghian1357@gmail.com

<sup>1</sup> Department of Civil Engineering, Faculty of Engineering, Estahban Branch, Islamic Azad University, Estahban, Iran

<sup>2</sup> Department of Civil Engineering, Faculty of Engineering, Shiraz Branch, Islamic Azad University, Shiraz, Iran

**Table 1** Summary of some of available TRMM and PERSIANN family satellite-derived precipitation products (Sun et al. 2018)

Data set	Spatial resolution	Frequency	Period	Data source
TRMM 3B42	0.25°	3-h	1998–2020	TMI, TRMM Combined Instrument, SSM/I, SSMIS, AMSR-E, AMSU-B, MHS and GEO IR
TRMM 3B43	0.25°	Monthly	1998–2020	TMI, TRMM Combined Instrument, SSM/I, SSMIS, AMSR-E, AMSU-B, MHS and GEO IR
PERSIANN	0.25°	Hourly	2000–present	
PERSIANN-CSS	0.04°	Hourly	2003–present	Meteosat, GOES, GMS, SSM/I, polar/near polar precipitation radar, TMI, AMSR
PERSIANN-CDR	0.25°	3-h	1983–present	GOES 8, GOES 10, GMS-5, Metsat-6 and Metsat-7, TRMM, NOAA 15, 16, 17, DMSP F13, F14, F15

application, ground, radar and satellite-based precipitation products are widely used in watershed models (Gilewski and Nawalany 2018; Price et al. 2014), and various comparative indicators have been used to evaluate the effect of the input data source (rain gauges, radars or satellite-derived products) on the performance of simulations employ such data (Gilewski 2021; Gupta et al. 2009; Zubieta et al. 2015). The rain gauges estimate point precipitation directly at the Earth's surface, and no complicated procedure is needed to prepare data to be used. However, in spite of the greater reliability, such measurements, for lack of observations (i.e., low spatiotemporal resolution), often do not fulfill all the requirements in many hydrological models. In addition to scarcity of ground-based rainfall observations, the extravagant prices for construction and maintenance of rain gauge stations make achieved data unnecessarily expensive. Therefore, currently, usage of air-based products to approximate rainfall parameters gradually increases in many environmental simulations, and high confidence in accuracy of such data is vastly needed.

Satellite systems have been used to measure atmospheric parameters since the early 1960s. In the primary systems, only the produced images of clouds and their comparison with meteorological observations were the indicators for estimating atmospheric parameters, but in the next steps, satellites were equipped with more advanced sensors. The sensors mainly categorized into three classes: visible/IR (VIS/IR) sensors on geostationary (GEO) and low Earth orbit (LEO) satellites, passive MW (PMW) sensors on LEO satellites, and active MW sensors on LEO satellites (Michaelides et al. 2009; Prigent 2010). Each of the sensors can be used individually or combined to develop procedures including the VIS/IR-based methods, active and passive MW techniques, and compound VIS/IR and MW approaches to estimate precipitation (Kidd and Levizzani 2011). Sensors and precipitation deriving methods are continuously being improved in order to raise the accuracy, certainty and reliability level of remotely sensed rainfall measurement.

Among a number of satellite-based rainfall monitoring programs, Tropical Rainfall Measuring Mission (TRMM),

Global Precipitation Measurement (GPM), and Precipitation Estimation from Remotely Sensed Information using Artificial Neural Networks (PERSIANN) are three well-known, widely used and evolving processes that have attracted a great deal of research. TRMM was a joint space mission sponsored by NASA and Japan Aerospace Exploration Agency (JAXA) from 1997 to 2015, and afterward, with the cooperation of an association of international space agencies, its activities are continued using modern satellite technologies equipped with advanced sensors under the name of GPM. Besides TRMM and GPM, PERSIANN is a soft-computing-based approach to estimate rainfall, developed by Center for Hydrometeorology and Remote Sensing (CHRS) at the University of California for global precipitation data gathering over the last two decades.

TRMM and PERSIANN families include some satellite-derived precipitation data sets which provide rainfall data at different spatiotemporal resolutions (Table 1). Numerous studies on application of satellite-derived precipitation products in hydrology are about evaluation of validation and/or reliability of such retrieved data over global or local scales, some of which are referred to on the map shown in Fig. 1. In these studies, it is tried to assess the quality of the products, through quantification of the uncertainties in the reprocessed data or the retrieval algorithms used to regenerate such data.

Several quantitative indices are used to validate the satellite-based precipitation products. The measures range from the elementary pairwise metrics such as correlation coefficient, the bias and the root-mean-square deviation (Camici et al. 2018; Chen et al. 2013a, b; Darand et al. 2017; Gao et al. 2018) to numerical results of advanced validation approaches such as triple collocation analysis (Li et al. 2018; Lu et al. 2021), consistency through process models and spectral methods (Nourani et al. 2013). Among the metrics, all pairwise methods are calculated between two data sets, both of which are subject to errors. However, for validation purposes, they are commonly calculated with respect to a presupposed error-free reference data. Therefore, they are assumed to represent an estimate of the various uncertainty aspects of the data set under validation. Furthermore, beyond



**Fig. 1** Continental distribution of some research on TRMM and PERSIANN satellite precipitation validation

the use of elementary validation metrics, probability distribution function (pdf) intercomparison and the stability of monitoring satellite data records are other methods to evaluate trustworthiness of satellite-based precipitation products (Dinku et al. 2008; Tan and Santo 2018).

In addition to “verification” or “validation” of satellite-based precipitation products, many studies conducted to evaluate the “reliability” of such data are based on the ability to detect precipitation (Gumindoga et al. 2019; Masood et al. 2020; Mosaffa et al. 2020). Probability of detection (POD), false alarm ratio (FAR), and critical success index (CSI) are three classified statistical indicators which are applied to evaluate the ability to detect actual precipitation events as the reliability of the satellite precipitation data (Paredes Trejo et al. 2016). POD represents the proportion of correctly detected precipitation events, FAR represents the proportion of missed precipitation events, and CSI comprehensively reflects the ability of satellite precipitation data to detect actual precipitation. However, these indicators often deal with the ability of detecting or not detecting rainfall events, but reliability of detected events is not considered.

Generally, for satellite-derived precipitation data, the term “reliability” refers to the consistency of the products in quality of the precipitation detection. In other words, the above-mentioned indicators just deal with the ability–inability in detection of rainfall event as well as accuracy–inaccuracy of satellite-derived databases and the relative quality of the retrieved data is not considered. For example, while the observed daily rainfall intensity is  $3 \text{ mm day}^{-1}$ , the aforementioned reliability attributes reflect the same values

for both corresponding satellite-derived measurements  $4.5 \text{ mm day}^{-1}$  and  $10 \text{ mm day}^{-1}$ , and the difference in reliability between these two values is not highlighted properly.

The “certainty” of the amount of rainfall retrieved by satellites is another issue to evaluate the correct performance of satellites and the applicability of algorithms used in the production of precipitation data. Error analysis is commonly used to calculate the certainty of rainfall values obtained from satellite data (AghaKouchak et al. 2012). Here, satellite-based precipitation estimation error characteristics quantified, and the influence of the error propagation into hydrological simulation is assessed. The indicators used for quantification of the error of satellite-based precipitation data are mainly the same metrics used for validation (e.g., bias), and most studies do not draw a clear line between certainty and validity of satellite-based precipitation data.

To address the critical shortcomings of many studies on evaluation of satellite-based precipitation products, it should be noted that in most of them, the data obtained from rainfall estimating algorithms which process the signals sent from satellites have been compared with deterministic and error-free ground- or radar-based data. Therefore, the randomness characteristic of ground-based data is usually ignored, and to explain the probability in the calculated comparing indicators, no probability conditions have been assigned to them.

In this paper, in the first step, all data, whether satellite-based or ground-based, are considered as random variables. For this purpose, appropriate probability density functions are assigned to them, and most computations are based on analysis and comparison of random variables. Furthermore,

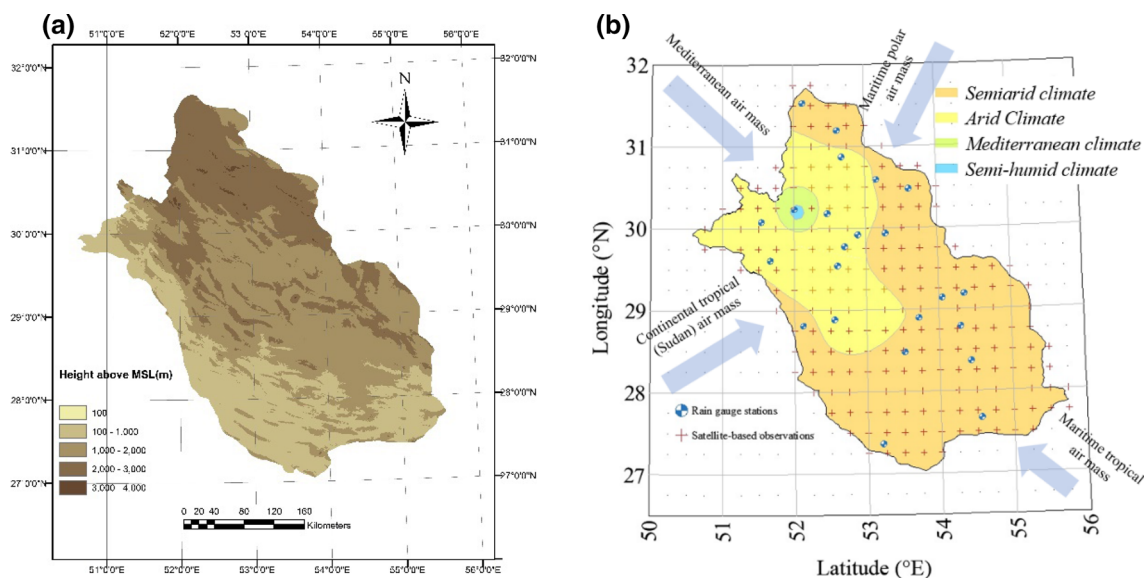


**Fig. 2** **a** Elevation map of the study area, **b** spatial distribution of available ground-based and satellite-based observation, regional climate division, and direction of air masses affecting the study area

some statistical validation approaches besides a reliability index and Shannon's entropy as a measure for uncertainty are employed to evaluate and compare TRMM 3B42RT (is called TRMM in this study) and PERSIANN daily precipitation data, as two databases represent their family in a large number of studies in which the quality of the SDDPD is assessed, over Fars Province, Iran. The study area has mainly arid and semiarid climates, and the comparison and validation results are reported separately for each climate. The study tries to narrow the focus of the investigation to concentrate on error resources. In other words, besides the answer to this question that whether the satellite-derived data are valid, reliable and/or certain, it is tried to find the measures for constituent parts of data collection such as several rainfall intensities, and pave the way for accurately detecting the errors and rectify them for probable further applications.

This is the first of a series of papers aimed at incorporating into employment of reliable SDDPD in hydrometeorological applications, such as rain gauge network design, IDF curve development and spatiotemporal forecasting approximation in the study area. The aforementioned models, however, require long-term historical rainfall observations, whereas lack of high-temporal-resolution rainfall records (e.g., sub-daily) often results in less satisfactory outcomes. High-temporal-resolution rainfall observation, however, is often a luxury for many regions due to the high cost, confidentiality, time-consuming procedures involved in data acquisition and sharing, etc., and as substitutions to the in situ rainfall measurement, reliable and interpretable satellite-based precipitation products meet the fundamental requirements in case of data scarcity. Consequently, the

results of this paper will be considered as the base of the foregoing hydrological simulations.

## Study area and data

### Study area

Fars province, as the study area, is located nearly in southwestern part of Iran ( $27^{\circ}$ – $32^{\circ}$  N,  $50^{\circ}$ – $55^{\circ}$  E) with a total area of  $122,608 \text{ km}^2$ . As shown in Fig. 2a, the study area, contains mountainous regions, mainly situated in northern and northwestern sector of the province, in which 54% is covered with elevations more than 1500 m above M.S.L. However, the southern and eastern parts of the study area are covered by flat lands (southern coastal plains and eastern deserts) with average slopes less than 5% and elevation less than 1000 m above M.S.L. Therefore, various landform classes can be found in the study area.

In addition to the topographical setting, three air masses including maritime polar, Mediterranean and continental tropical (also known as Sudan) normally influence the study area in the wet period (November–April), and the maritime tropical air mass only influences the study area in the dry period, May–October (Heydarizad et al. 2019; Javanmard et al. 2010). Among the masses, Mediterranean is one of the most active air masses and affects almost all parts of the study area. Mediterranean air mass supplies moisture from the Mediterranean Sea and the Atlantic Ocean, and to a lesser extent the Black Sea (Heydarizad et al. 2018). The maritime polar air mass dominantly influences the study area

**Table 2** Climatological (aridity) classification and the related precipitation and temperature information of the selected synoptic stations in the study area

Station code	Geographical coordinates		Elevation (m)	AAT <sup>+</sup> (°C)	AAP <sup>++</sup> (mm)	IDM <sup>+++</sup>	Climatological classification
	Longitude	Latitude					
40,848	52°36'10"	29°32'39"	1484	18.1	317.49	11.3	Semiarid
99,566	52°00'24"	30°14'03"	2201	14.7	648.65	26.3	Semi-humid
40,818	52°36'42"	31°11'54"	2030	14.4	134.9	5.5	Arid
99,646	53°31'02"	28°28'58"	1082	20.8	276.1	9.0	Arid
40,847	52°42'15"	29°46'39"	1596	16.5	303.71	11.5	Semiarid
40,844	52°27'54"	30°10'59"	1650	17.7	457.14	16.5	Semiarid
99,580	51°32'39"	30°04'46"	972	21.2	458.1	14.7	Semiarid
88,190	53°12'12"	27°21'52"	405	25.6	212.25	6.0	Arid
40,861	51°39'54"	29°36'26"	860	23.1	358.3	10.8	Semiarid
99,561	53°36'32"	30°28'34"	2231	13.8	215.12	9.0	Arid
40,828	52°40'32"	30°52'09"	2300	13.0	319.81	13.9	Semiarid
40,855	53°09'23"	30°35'27"	2251	12.1	204.05	9.2	Arid
40,869	54°21'07"	29°11'12"	1632	19.5	197.12	6.7	Arid
40,862	54°17'46"	28°47'25"	1098	22.2	262.26	8.1	Arid
99,607	54°02'54"	29°08'25"	1690	17.4	253.86	9.3	Arid
40,859	53°43'10"	28°53'56"	1288	19.4	286.01	9.7	Arid
40,873	54°22'29"	27°40'12"	792	23.8	210.06	6.2	Arid
99,575	52°53'21"	29°55'11"	1605	17.5	291.68	10.6	Semiarid
99,516	52°07'42"	31°31'47"	2188	13.8	151.6	6.4	Arid
99,579	53°16'46"	29°56'08"	1703	18.4	236.4	8.3	Arid
99,590	54°25'44"	28°21'55"	1029	23.2	216.9	6.5	Arid
99,630	52°33'06"	28°53'09"	1362	20.7	377.2	12.3	Semiarid
40,864	52°07'09"	28°48'47"	782	22.2	272.3	8.5	Arid

<sup>+</sup>average annual temperature, <sup>++</sup>average annual precipitation, <sup>+++</sup>De Martonne aridity Index

during December, January, and February, while the Mediterranean air mass dominantly influences the study area during March and April. The continental tropical air mass enters from the south and affects most parts of the study area (like the Mediterranean air mass), but affects the south most strongly. The continental tropical air mass transports a considerable amount of moisture from the Persian Gulf, the Red Sea and the Arabian Sea. The continental tropical air mass has a crucial role in the rainfall in the study area during all of the wet period. However, the summer precipitation southeast of the study area is sometimes influenced by the maritime tropical air mass. The maritime tropical air mass supplies moisture from the Arabian Sea and the Indian Ocean to southeast and south of the study area (see Fig. 2b).

Topographical setting (elevation differences and slope characteristics) and the arriving air mass systems in the study area control the regional climate conditions. Generally, several quantitative measures are focused to categorize the climate conditions based on different climatic elements: precipitations only, for example SPI<sup>1</sup> (Caloiero et al.

2018) and ASP<sup>2</sup> (Liu et al. 2016), besides temperature and precipitations, for instance, IDM<sup>3</sup> (Pellicone et al. 2019; Tabari et al. 2014) and IP<sup>4</sup> (Baltas 2007). Among the indices, although De Martonne aridity Index is one of the oldest aridity/humidity indices, because of its efficiency and relevance in relation to the arid/humid climate classification, in recent years, it was still used with good results worldwide in order to identify dry/humid conditions of different regions (Emadodin et al. 2019; Pellicone et al. 2019; Zarghami et al. 2011) and is employed in this study. The index may be calculated both on annual and on shorter period basis. For annual values, it may be calculated as presented below:

$$DMI = \frac{P_{aa}}{T_{aa} + 10}, \quad (1)$$

<sup>2</sup> Anomaly Standardized Precipitation.

<sup>3</sup> De Martonne aridity Index.

<sup>4</sup> Pinna combinative Index.

<sup>1</sup> Standardized Precipitation Index.

where  $P_{aa}$  is the annual amount of precipitation (in millimeters) and  $T_{aa}$  is the mean annual air temperature (in degree Celsius).

Figure 2b also displays regional climate classification, with regard to De Martonne aridity Index, over the study area based on the data gathered from the meteorological stations shown in Table 2. The spatial distribution of the aridity index calculated for annual values reveals that the driest regions in the study area are located in the southeastern and northern parts, which are included hot arid climate southern coastal plains and eastern deserts, also cold arid climate northern mountainous section. The remaining areas in central and western parts have mainly semiarid climate. However, the only stations close to the northwestern boundary recorded values specific to semi-humid climates.

## Data set

The reference data sets employed in the present work are based on the daily rainfall observations derived from 23 synoptic stations (Table 2 and Fig. 2). The synoptic station data were provided by Iran Meteorological Organization (IMO), and the recording period of the stations varied in duration, but all had data from 2000 to 2020 which are completely compatible with period of available SDDPD. The spatial distribution of the synoptic gauge stations over the study area is deducible from the map in Fig. 2b, and it is not difficult to qualitatively infer that most of the stations spread uniformly in the study area.

In addition to ground-based observations, TRMM 3B42RT and PERSIANN are a couple of general satellite-based precipitation data are used in this study. The TRMM 3B42RT precipitation output comprises  $0.25^\circ \times 0.25^\circ$  grid cells (about 25 km  $\times$  30 km in location of the study area) for every 3 h, with spatial extent covering a global belt ( $-180^\circ\text{W}$  to  $180^\circ\text{E}$ ) extending from  $50^\circ\text{S}$  to  $50^\circ\text{N}$  latitude. Besides TRMM satellite-based precipitation products, SDPPs based on PERSIANN, also, compute an estimate of rainfall rate at each  $0.25^\circ \times 0.25^\circ$  pixels, but, for every 1 h. As TRMM 3B42 data, PERSIANN rainfall product covers  $50^\circ\text{S}$  to  $50^\circ\text{N}$  globally. The utilized TRMM 3B42 and PERSIANN data in this paper were covering the study area from 2000 to end of 2019.

UTC offset and probable delay in recording observations are crucial issues in recovering daily data hour-based information (which is not much focused in the literature). For example, to obtain a daily-scale 3B42 product, the precipitation measurements from eight three-hourly products (00:00 UTC, 03:00 UTC, 06:00 UTC, 09:00 UTC, 12:00 UTC, 15:00 UTC, 18:00 UTC, and 21:00 UTC) of a specific date were accumulated and multiplied by a factor of 3. Since the precipitation gauges in the study area measure the daily precipitation with regard to local time, a time calibration

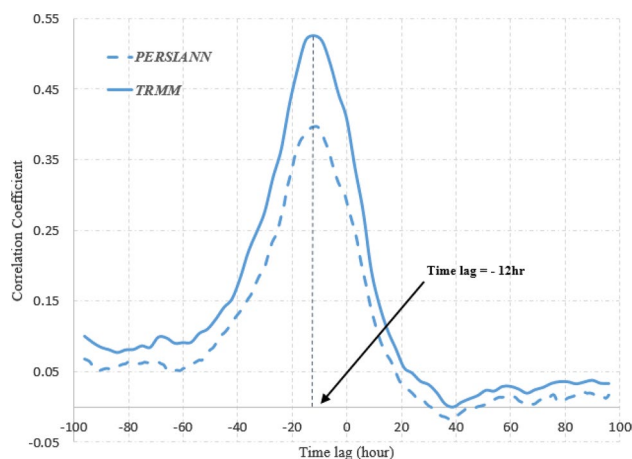


**Fig. 3** Correlation coefficient between SDPPs and ground-based observations considering several time lags

is required for the matter. Figure 3 shows average correlation coefficient between daily precipitation of rain gauge observations and the generated values from hourly-scale data derived from the TRMM and PERSIANN satellites. It is clear from the figure that considering a delay between, about 12 h, beginning hour in a day to generate daily precipitation data from hourly (for PERSIANN) and/or three-hourly (for TRMM) products yield to the highest correlation coefficient and probably provide more efficient results. Therefore, in this study, the daily-scale satellite-derived products were synchronized with ground-based observations from shifting the time 12 h earlier to compensate the time difference between local and standard time, and any probable delay in data reporting.

## Methodology

The validity, reliability and certainty of daily precipitation data retrieved from TRMM and PERSIANN databases are evaluated by comparing them with IMO ground-based observations in selected synoptic stations during the period spanning from 2000 to 2019, corresponding to availability of almost complete data sets during these years. A detailed comparison of the data sets is provided in different climates of the study area, to assess the relationship between climate conditions and the quality of the SDDPD. To achieve these goals, a straightforward procedure is established from taking the following steps:

1. Choose a method to divide the study area into regions with the homogeneous climate conditions or similar climatic indicators:

Climatic classifications is mainly used to reflect the average spatial climatic characteristics of a region (Geng

**Table 3** Type of climate according to the De Martonne aridity Index (IDM)

Climate type	$I_{DM}$ value
Arid	$I_{DM} < 10$
Semiarid	$10 \leq I_{DM} < 20$
Mediterranean	$20 \leq I_{DM} < 24$
Semi-humid	$24 \leq I_{DM} < 28$
Humid	$24 \leq I_{DM} < 35$
Very humid	$35 \leq I_{DM} < 55$
Extremely humid	$I_{DM} \geq 55$

et al. 2014). Various climatic classification models based on meteorological parameter processing approaches are found in the literature (De Martonne 1926; Gadgil and Narayana Iyengar 1980; Stamp and Wooldridge 1951; Thornthwaite 1955). Among the methods, De Martonne climatic classification approach has been used in many environmental studies in recent decades, indicating that although this index is one of the oldest climate indices, but it is still worldwide used with logical results in order to mirror climate conditions of different regions (Emadodin et al. 2019; Pellicone et al. 2019). Therefore, based on the simplicity and efficiency of the De Martonne aridity Index, this approach is chosen for dividing the study area into climatic subregions (refer to Eq. 1 and Table 3).

2. *Select conventional diagnostic statistics to quantify the accuracy of the PERSIANN and TRMM daily precipitation:*

Six parameters are used to measure the precision of the satellite-derived data: the Pearson and the Spearman's rank correlation coefficients (Zou et al. 2003), the root-mean-square error (Gupta et al. 2008, 2009), the mean error, mean absolute error, relative bias and Kolmogorov–Smirnov statistic (Zhang et al. 2011). The values for the first five parameters are calculated by the following equations:

$$\text{Pearson correlation coefficient} : \frac{\text{cov}(S, G)}{\sigma_S \sigma_G}, \quad (2)$$

$$\text{Spearman's rank correlation coefficient} : \frac{\text{cov}(S_r, G_r)}{\sigma_{S_r} \sigma_{G_r}}, \quad (3)$$

$$\begin{aligned} \text{Mean error} &: \bar{E} \\ E_i = S_i - G_i & \quad \text{Mean absolute error} : \overline{|E|}, \quad (4) \\ \text{Relative Bias} &: \frac{\bar{E}}{G} \times 100 \end{aligned}$$

where  $S$  and  $G$  are satellite-derived precipitation data and the observed precipitation from gauges,  $S_r$  and  $G_r$  are rank variables of the previously mentioned parameters, and  $S_i$  and  $G_i$  are corresponding daily satellite-derived precipitation data and the rain gauge observations. In addition, the Kolmogorov–Smirnov statistic quantifies a distance between the cumulative distribution function of the satellite-derived precipitation data and the cumulative distribution function of the rain gauge observations considered as reference distribution (Bityukov et al. 2016).

3. *Employ the statistical concept of consistency to determine reliability degree of PERSIANN and TRMM daily precipitation.*

Reliability and the probability of failure are on both sides of balance scale so that the lowering of one causes the rising of the other (Biroolini 2017). For the satellite-derived precipitation measurements, failure means incorrect retrieval of the amount of rainfall sent by satellite signals which is directly related to the value of the acceptable error threshold. In other words, error in a given interval, known as threshold, is considered to be insignificant, and the corresponding amount of satellite-derived precipitation is considered to be acceptable (reliable). However, if the error value is outside the negligible error range, the related precipitation value is unacceptable (failure). It is obvious that the number of acceptable rainfall amounts, and consequently level of reliability, increases with the expansion of the acceptable error range; however, the relationship between the rate of change in the level of reliability and the values of the acceptable error range has received less attention.

Statistically, error probability distribution function is, also, another basic constituent of the reliability concept. The function is derived from empirical distribution function of the generated samples based on SDDPD. Furthermore, the procedure for modeling the distribution function requires a goodness-of-fit test. Hence, choosing an appropriate type of distribution test function and fitting procedure, besides providing the error structure of satellite-derived precipitation values are integral parts of reliability analysis.

4. *Introduce an effective uncertainty index to imply the viability of the PERSIANN and TRMM SDPPs.*

Uncertainty analysis of satellite-derived precipitation products is a computational process of quantitatively analyzing possible errors and estimating of the total uncertainty of a measurement. Conventionally, quantifying uncertainty in satellite-derived precipitation products, accuracy of data is determined; however, most of the traditional disinformative uncertainty indicators are not able to identify source of data uncertainty. Therefore, to tackle the problem, entropy is considered

as an effective measure to represent uncertainty of data (Amarocho and Espildora 1973; Robinson 2008).

For more clarification, here an illustrative example is provided. Suppose the real value for a parameter to be 10. The value was observed by a couple of devices, in which the first observed values were 9, 11, 12, and 8. On the other hand, the second device recorded observation values were 14, 14, 14, 14. Here, mean error (bias), as one of the traditional uncertainty indices, related to the first device is 0; however, the mean error of the second device is 4. Traditionally, the uncertainty index of the second device is higher, but the error was spread uniformly in all the observations and may remove hardly. However, the error can be easily detected and removed in the second device.

Entropy is a measure of redundancy. The relative entropy gives a comparison between two probabilistic systems and typically measures the actual entropy to the maximal possible entropy. It is the relative entropy that has played the key role in determining the uncertainty indices of this study.

The above steps require some tools which are explained as follows:

### Statistical analysis

A purposive approach to the probabilistic concepts produces some meaningful results that can be effectively utilized in logical interpretation of such subjects. The methods are comprised mainly of suitable probability density functions (pdfs) in addition to effective analytic strategies and reasonably inferring plans. These pdfs represent random variables fairly well and remove noises from data effectively. Besides, well-organized processing techniques provide deducible results that enable to classify data, clarify the current situation and establish intellectual foundations for forecasting procedures. Therefore, analyzing the events including random variables requires careful selection of constituents of statistical analysis procedure to form objective judgment on the measures.

Proper probabilistic evaluation of satellite-derived precipitation data by comparing them with rain gauge observations, while both are considered to be random variables, requires some essential statistical tools. Accordingly, pdfs of satellite-derived precipitation data and rain gauge observations, as the basis for many statistical analyses, are better to be established in early stages of the study. Establishment of pdfs is to identify the type of proper shape and define its calibrating parameters utilizing a conscious fitting policy with non-debatable measures.

For averaged daily precipitation, a gamma distribution is commonly used for describing rainfall statistics (Martinez-Villalobos and Neelin 2019). The function is given by:

$$f(x) = \frac{\beta^\alpha}{\Gamma(x)} x^{\alpha-1} e^{-\beta x}, \quad (5)$$

where  $\alpha$  is the shape parameter,  $\beta$  the rate parameter, and  $x$  represents daily averaged precipitation. For daily precipitation, shape and rate parameters are applicable metrics to control the probability of light and moderate daily precipitation sums, and represent changes of the extremes, respectively (Wilby and Wigley 2002).

### Reliability analysis

For satellite-derived precipitation data, most of the research focuses on accuracy of the measurements, while their consistency is not highly regarded. Increasing the accuracy of the data is a direct consequence of the error reduction, while their consistency achievement is essence of error organization. So, profound knowledge to error nature of satellite precipitation data increases the “reliability” of their utilization in hydrological models. Statistically, the reliability may be defined as follows:

$$R(E) = \Pr(-E \leq x \leq E) = \int_{-E}^{+E} f_e(x) dx, \quad (6)$$

where  $E$  is the acceptable error domain of satellite data and  $f_e(x)$  is pdf of the satellite data error. The measure indicates the trustworthiness degree of the data with regard to predefined probable deviation from the ground rain gauge observations.

### Shannon entropy analysis

Error uncertainty of the satellite data may be utilized as a measure to evaluate their performance. Generally, uncertain data are data that contain noises that which make them deviate from the correct, intended or original values. Hence, calculating error uncertainty of the satellite daily rainfall data seems to be an appropriate way to delineate of their applicability for several usages.

Entropy is an encapsulation of the rather vague notions of disorder or chaos, uncertainty or randomness. The measure implies the degree of uncertainty to the values of data if the process takes place for errors. For more details, consider the Shannon entropy definition of data error:



$$H(\text{ERR}) = \begin{cases} \sum_{i=1}^N -P(x_i) \ln P(x_i), & \text{empirical data set} \\ \int P(e) \ln P(e) de, & \text{the modeled pdf} \end{cases}, \quad (7)$$

where, for analyzing empirical data sets,  $N$  is number of error domains. Besides,  $x_i = \{x \in X : e_i < \text{Err}(x) < e_{i+1}\}$  where  $X$  is data set,  $\text{Err}(x)$  is error value for  $x$ , and  $e_-$  are sequential predefined errors. In addition, for the modeled pdf,  $P(e)$  is probability of error  $e$ . For both cases,  $H(\text{ERR})$  represents uncertainty of errors. Lower values of  $H(E)$  imply certainty of errors more and increase the ability to identify and remove errors.

It can be shown that, for empirical data set, the value of  $H(E)$  is maximum when all the  $x_i$  are equally probable, that is, when the outcome has maximum uncertainty. In this case, the entropy becomes:

$$H_{\max}(\text{ERR}) = \ln N. \quad (8)$$

At the other extreme, when all outcomes except one have zero probability,  $H(E)$  vanishes, which corresponds to absolute certainty. On the other hand, for modeled pdf, with respect to Appendix, while normal skew distribution function is used to simulate the extreme entropy the values are:

$$\begin{aligned} H_{\max}(\text{ERR}) &= H_{\text{ND}} \\ H_{\min}(\text{ERR}) &= H_{\text{ND}} - \ln 2^2 \end{aligned} \quad (9)$$

where  $H_{\text{ND}}$  is entropy of normally distributed function.

For skewed normal distribution function (Eq. 11), the entropy is calculated as (Arellano-Valle et al. 2013):

$$H(E) = \frac{1}{2} + \frac{1}{2} \ln(2\pi w^2) - E \left\{ \ln \left[ 1 + \text{erf} \left( \alpha \frac{(x - \xi)}{w} \right) \right] \right\}. \quad (10)$$

## Results and discussion

The focus of this study is to evaluate the validity, reliability and uncertainty of two well-known SDDPD called TRMM (TRMM 3B42RT) and PERSIANN. It should be noted that indicators for the aforementioned concepts can be defined based on different viewpoints. In this paper, various statistical procedures are used to assess these indicators that are mentioned in detail in the previous section.

Table 4 reports shape and rate parameters of the gamma distribution function for rain gauge observations, PERSIANN and TRMM explained in Eq. 5. In Table 4 (and others), gray rows represent stations located in arid region, while the values in orange and green rows are related to stations placed in semiarid and semi-humid climates, respectively. The parameters were calibrated from optimizing the

modeled probability distribution to the sample to achieve minimum distance in Kolmogorov–Smirnov test which can be found in this table. Besides, maximum vertical distance between cumulative distribution function (cdf) of daily rain gauge observations and corresponding satellite-derived data are shown, which are used in performing a Kolmogorov–Smirnov test for the null hypothesis that rain gauge observations and TRMM or PERSIANN are reasonably from the same distribution function (Teegavarapu 2019). In addition to the parameters of the pdfs, some common cross-validating attributes are presented in Table 4. The linear association between the satellite-derived data sets and rain gauge observations is evaluated using Pearson and Spearman rank correlation coefficients (Eqs. 2 and 3). Bias in the mean daily precipitation of all data sets is estimated with mean error (Eq. 4). The mean absolute error (Eq. 4) and the root-mean-square error (RMSE) are used to measure the average magnitude of the errors, with the difference that RMSE gives greater weight to the larger errors relative to MAE. Finally, with the relative bias (Eq. 4) the mean error was scaled with respect to the mean precipitation of the gauge observations.

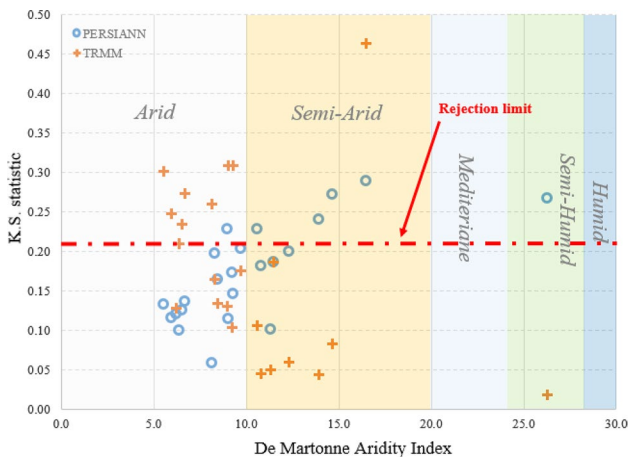
Precipitation observations and satellite data are considered as random variables. The probability distribution function can be used to validate the rainfall amount distribution and the error dependence on precipitation rate for satellite estimates (Chen et al. 2013b; Tian et al. 2009). This kind of evaluation also offers insight into error dependence on precipitation rate and the potential impact of the error on hydrological applications. The K–S statistic values for each set of data (rain gauge observations, PERSIANN and TRMM) confirm a good enough fit in all cases. However, Fig. 4 indicates that the metric denotes quantitative comparison of satellite data with rain gauge observations, somehow depends on the climate of the region. Since the hypothesis is rejected if the K–S statistic is higher than the critical value 0.20517 at a 95% significance level of confidence (Langat et al. 2019), regarding the figure, TRMM detects rainfall more efficiently in wetter regions than the PERSIANN satellite. But, for arid regions, the pdf similarities of PERSIANN and rain gauge observations are more considerable.

Figure 5 shows some statistical distinguishing indices for validation of PERSIANN and TRMM in several climates in the study area. Pearson and Spearman rank correlation coefficients do not show a clear pattern for any of the satellites and regions. However, the values of ME and BIAS lead to the conclusion that PERSIANN almost underestimates the rainfall daily rates while TRMM overestimates the value mainly in semiarid regions. In addition, the figures indicate that the “pattern of the errors” for PERSIANN is more organized. For instance, absolute values for RMSE, ME, MAE, and BIAS gradually become more substantial with increasing the De Martonne aridity Index, although no significant pattern can be found for TRMM. The pattern may

**Table 4** Rain gauge daily observations, PERSIANN and TRMM satellite daily data estimated parameters summary of gamma probability distribution

Station code	RDGO			PERSIANN			TRMM			K-S statistic(PERSIANN-rain gauges)	K-S statistic (TRMM-rain gauges)	Pearson correlation coefficient	
	$\alpha$	$\beta$	K-S Stat.	$\alpha$	$\beta$	K-S Stat.	$\alpha$	$\beta$	K-S Stat.			RGDO-PERSSIANN	RGDO-TRMM
40848	0.40	0.09	0.06	0.55	0.19	0.03	0.40	0.11	0.01	0.101	0.050	0.37	0.60
99566	0.44	0.05	0.02	0.62	0.22	0.03	0.44	0.05	0.02	0.267	0.018	0.33	0.54
40818	0.41	0.19	0.04	0.67	0.30	0.03	0.49	0.06	0.03	0.133	0.301	0.35	0.23
99646	0.51	0.06	0.03	0.55	0.18	0.03	0.85	0.10	0.03	0.228	0.131	0.41	0.65
40847	0.42	0.07	0.03	0.60	0.24	0.04	0.58	0.05	0.02	0.187	0.186	0.37	0.55
40844	0.50	0.06	0.03	0.58	0.23	0.03	0.42	0.40	0.10	0.289	0.463	0.36	0.59
99580	0.60	0.07	0.04	0.62	0.19	0.04	0.39	0.03	0.02	0.272	0.083	0.31	0.46
88190	0.40	0.06	0.03	0.56	0.16	0.04	1.21	0.21	0.07	0.116	0.248	0.35	0.55
40861	0.50	0.07	0.05	0.57	0.18	0.03	0.39	0.05	0.03	0.182	0.045	0.24	0.56
99561	0.40	0.13	0.05	0.70	0.36	0.04	0.94	0.16	0.03	0.115	0.309	0.35	0.26
40828	0.55	0.10	0.04	0.62	0.29	0.03	0.45	0.07	0.02	0.240	0.044	0.28	0.26
40855	0.52	0.13	0.04	0.64	0.32	0.04	0.53	0.09	0.03	0.173	0.104	0.33	0.24
40869	0.40	0.09	0.04	0.62	0.28	0.03	0.96	0.15	0.06	0.137	0.273	0.40	0.36
40862	0.40	0.10	0.07	0.55	0.18	0.03	0.82	0.12	0.02	0.059	0.260	0.41	0.52
99607	0.40	0.09	0.05	0.63	0.28	0.03	1.15	0.18	0.04	0.146	0.308	0.46	0.48
40859	0.41	0.06	0.02	0.57	0.21	0.03	0.75	0.09	0.03	0.204	0.176	0.45	0.59
40873	0.52	0.09	0.03	0.59	0.17	0.03	0.85	0.14	0.04	0.121	0.128	0.36	0.39
99575	0.50	0.08	0.04	0.59	0.25	0.03	0.47	0.05	0.02	0.228	0.106	0.40	0.54
99516	0.44	0.13	0.04	0.68	0.31	0.03	0.56	0.08	0.03	0.100	0.210	0.37	0.20
99579	0.40	0.07	0.04	0.66	0.30	0.04	0.60	0.07	0.03	0.198	0.165	0.40	0.54
99590	0.40	0.07	0.04	0.58	0.19	0.04	0.83	0.10	0.04	0.126	0.234	0.30	0.57
99630	0.40	0.05	0.03	0.57	0.20	0.04	0.54	0.10	0.03	0.200	0.060	0.26	0.57
40864	0.43	0.06	0.03	0.60	0.19	0.03	0.63	0.07	0.03	0.165	0.134	0.32	0.43

Station code	Spearman rank correlation coefficient		RMSE		ME		MAE		BIAS	
	RGDO-PERSSIANN	RGDO-TRMM	RGDO-PERSSIANN	RGDO-TRMM	RGDO-PERSSIANN	RGDO-TRMM	RGDO-PERSSIANN	RGDO-TRMM	RGDO-PERSSIANN	RGDO-TRMM
40848	0.12	0.02	8.86	7.32	-1.85	2.04	4.20	3.41	-43.72	118.72
99566	0.08	0.13	13.22	13.13	-4.77	-1.57	6.79	7.45	-66.03	-20.17
40818	-0.09	-0.17	4.65	11.45	0.31	1.86	2.35	4.76	19.54	82.39
99646	0.02	0.13	10.83	10.58	-1.81	-1.37	5.47	6.43	-36.21	-18.59
40847	0.09	0.17	8.43	12.87	-2.09	2.56	4.26	6.41	-48.36	52.24
40844	0.08	0.04	11.73	8.58	-3.86	0.07	5.89	3.04	-62.30	2.59
99580	0.10	0.22	11.52	17.49	-2.42	3.00	6.00	9.57	-40.71	41.72
88190	0.06	0.09	9.81	9.97	-0.62	1.80	4.71	5.54	-15.42	44.72
40861	0.08	0.26	11.33	13.68	-1.64	2.92	5.67	7.02	-32.51	55.36
99561	-0.13	-0.29	6.40	9.69	-1.04	1.07	3.13	4.99	-37.82	36.01
40828	-0.10	-0.18	8.84	13.72	-2.14	0.69	4.26	6.34	-53.48	16.07
40855	-0.08	-0.18	5.81	10.97	-0.70	1.54	3.14	5.37	-25.73	48.38
40869	-0.02	-0.11	6.66	8.95	-1.20	-0.65	3.32	5.05	-38.74	-15.40
40862	-0.01	0.13	8.65	9.10	-1.61	-1.21	4.16	4.80	-41.82	-24.57
99607	0.01	0.05	8.57	9.51	-2.12	-1.68	4.03	5.01	-51.33	-33.04
40859	0.04	0.08	9.59	10.34	-2.09	-1.04	4.68	5.81	-46.17	-16.93
40873	-0.05	-0.05	8.67	9.95	-0.45	-1.12	4.51	5.61	-12.60	-22.09
99575	0.07	0.14	8.14	12.59	-2.22	1.59	4.26	6.21	-50.52	30.50
99516	-0.15	-0.17	4.96	10.89	0.00	1.70	2.65	5.29	0.02	59.16
99579	0.02	0.10	7.43	10.51	-1.34	0.95	3.73	5.36	-37.28	20.48
99590	-0.03	0.11	9.58	9.68	-0.43	-1.43	4.78	5.28	-11.69	-25.02
99630	0.04	0.18	11.23	10.78	-1.66	0.23	5.28	5.70	-34.99	3.99
40864	0.04	0.17	10.11	11.67	0.03	1.91	4.86	6.42	0.81	37.07



**Fig. 4** Climatological evaluation of the Kolmogorov–Smirnov test metric for the null hypothesis that the precipitation time series at daily resolution of rain gauges is the same as satellite data

help for error-removal of data with several kinds of error-generating noises (Fig. 6).

To evaluate error distribution inherent features, Fig. 2 shows the sample frequency and the model of PERSIANN and TRMM data error distributions in four sample locations with available daily rain gauge observations. The skew-normal distribution function (O’Hagan and Leonard 1976) is utilized to model the empirical distribution in such a way that distance between the empirical distribution

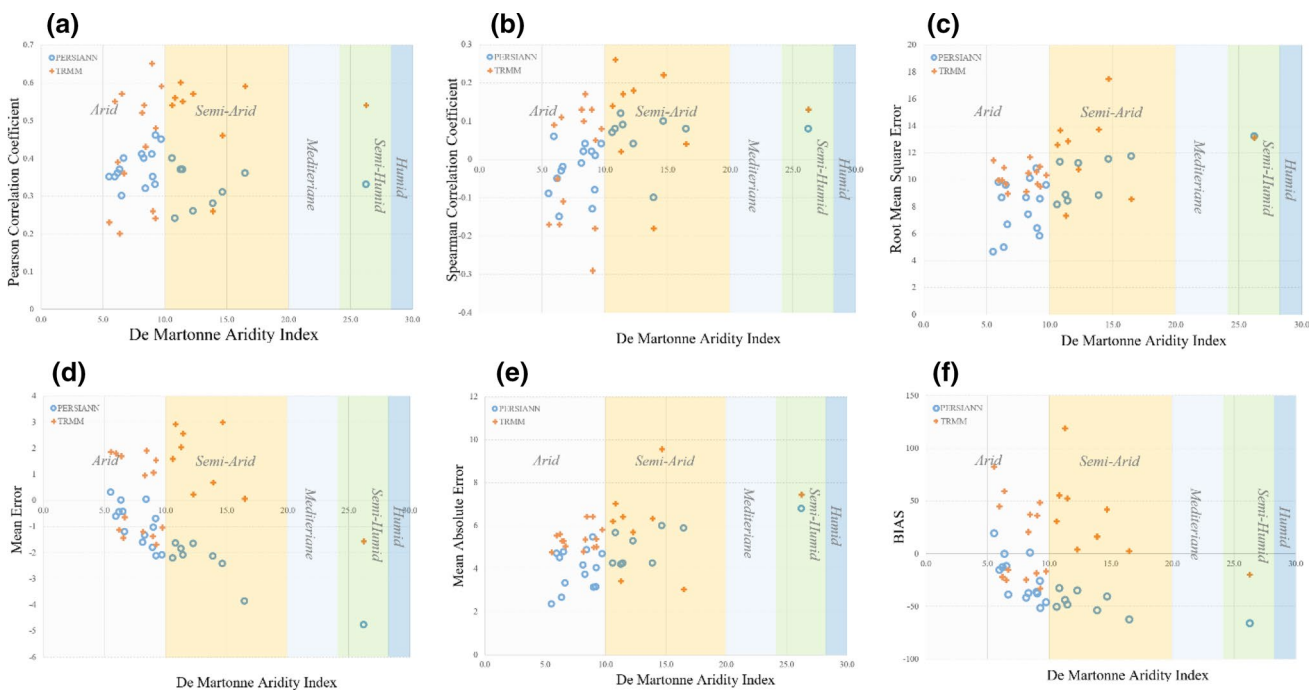
function of the sample and the cumulative distribution function of the reference distribution is minimized (the K–S stat. in Table 5 is used to indicate the minimum value which all reject the null hypothesis). The function model is as follows:

$$f(x) = \frac{2}{w\sqrt{2\pi}} e^{\frac{1}{2}\left(\frac{x-\xi}{w}\right)^2} \int_{-\infty}^{\alpha\left(\frac{x-\xi}{w}\right)} \frac{1}{\sqrt{2\pi}} e^{-\frac{t^2}{2}} dt, \quad (11)$$

where  $\alpha$  (shape parameter),  $w$  (scale parameter), and  $\xi$  (location parameter) are regulating parameters of the function. The distribution is right skewed if  $\alpha > 0$  and is left skewed if  $\alpha < 0$ . Regarding the parameters, mean, variance and skewness of the sample modeled by the aforementioned pdf are as follows:

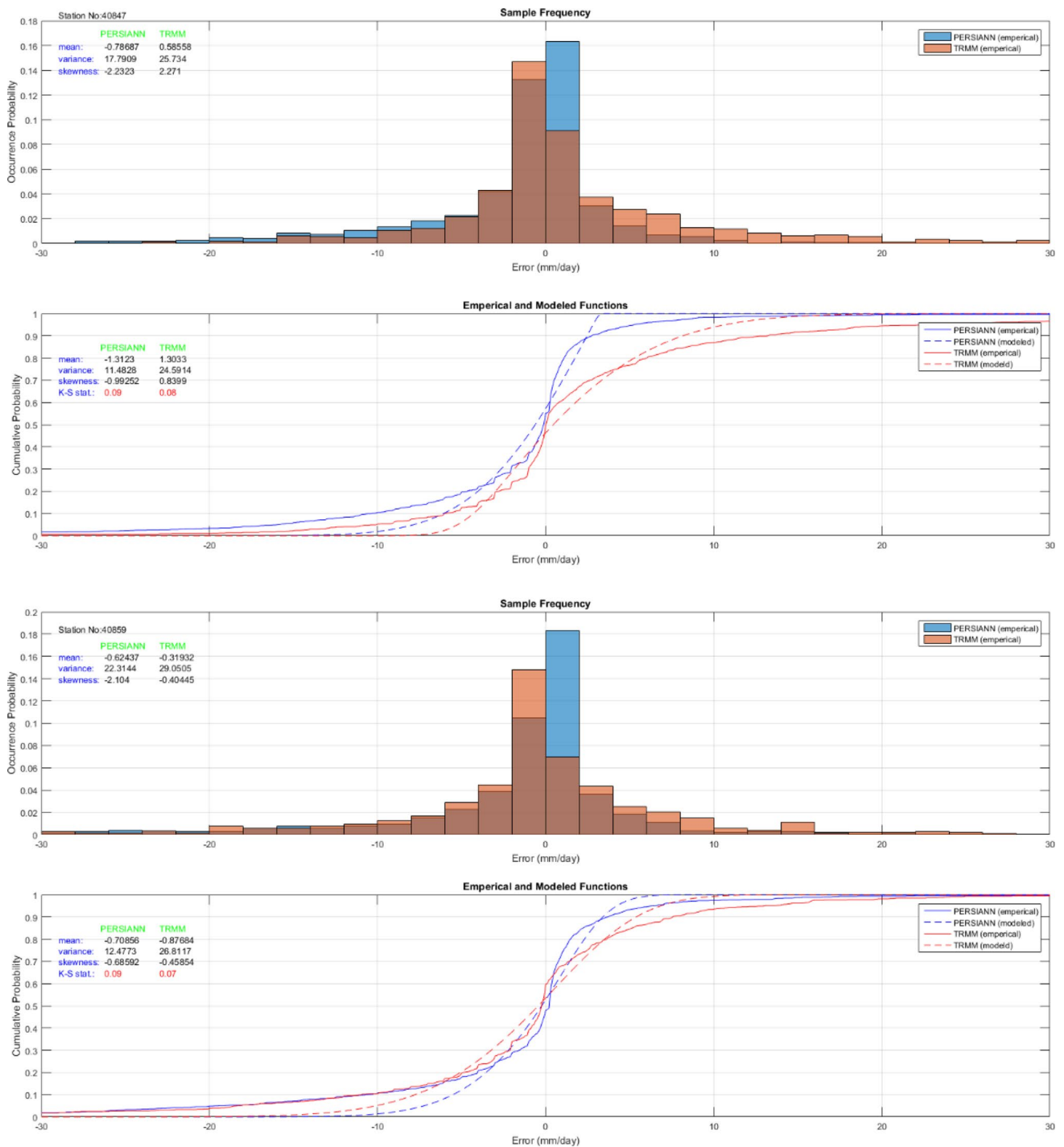
$$\begin{aligned} \text{Mean } (\mu) &= \xi + \delta \sqrt{\frac{2}{\pi}} \quad \text{where } \delta = \frac{\alpha}{\sqrt{1 + \alpha^2}} \\ \text{Variance } (\sigma^2) &= w^2 \left(1 - \frac{2\delta^2}{\pi}\right) \\ \text{Skewness } (\eta) &= \frac{4 - \pi}{2} \frac{\left(\delta \sqrt{\frac{2}{\pi}}\right)^3}{\left(1 - \frac{2\delta^2}{\pi}\right)^{\frac{3}{2}}}. \end{aligned} \quad (12)$$

Table 5 also contains the skew-normal model parameters besides the estimated mean, variance and skewness of



**Fig. 5** Statistical bi-cross-validation representation of the climatological validation of PERSIANN and TRMM daily precipitation estimates using the pixels with assimilated RGDO of Fars province:

**a** Pearson coefficient of correlation, **b** Spearman coefficient of rank correlation, **c** root-mean-square error (RMSE), **d** mean error (ME), **e** mean absolute error (MAE), and **f** relative bias (BIAS)



**Fig. 6** Rainfall daily intensity occurrence frequency in four typical stations

the simulated distribution (Eq. 12). The parameters were calculated establishing a genetic algorithm procedure to minimize the K–S statistics.

A reliability expression can be calculated by applying Eq. 11 in Eq. 6 as follows:

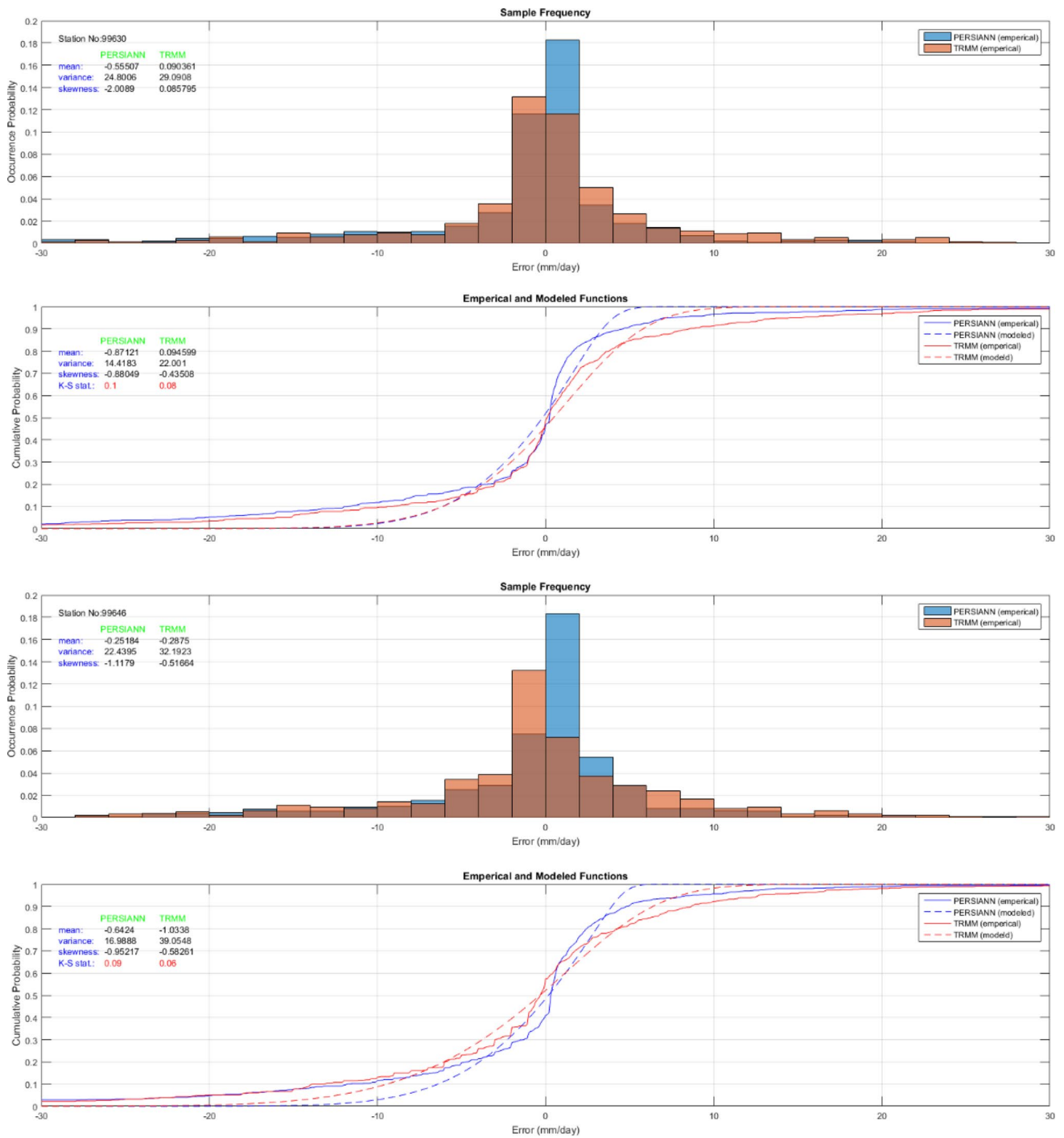
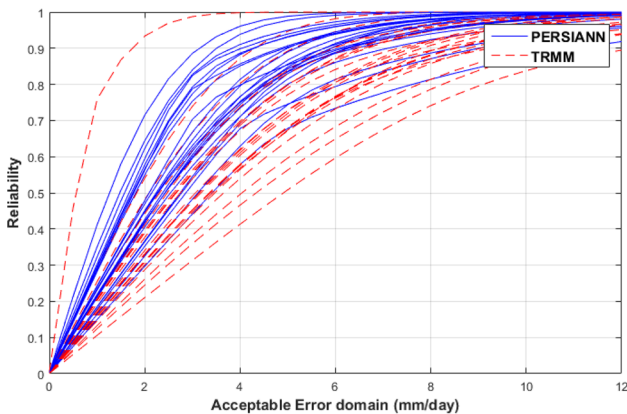


Fig. 6 (continued)

$$R(E) = \operatorname{erf}\left(\frac{E - \xi}{\sqrt{2}w}\right) + \operatorname{erf}\left(\frac{E + \xi}{\sqrt{2}w}\right) + T\left(\frac{E - \xi}{w}, \alpha\right) - T\left(\frac{E + \xi}{w}, \alpha\right), \tag{13}$$

**Table 5** The estimates of PERSIANN and TRMM satellite daily averaged data error distributions model parameters and the corresponding calculated simulated statistical measures (mean, variance, and skewness)

Station code	PERSIANN				TRMM				PERSIANN			TRMM		
	$\alpha$	$w$	$\xi$	K-S Stat.	$\alpha$	$w$	$\xi$	K-S Stat.	Mean ( $\mu$ )	Var. ( $\sigma^2$ )	Skew. ( $\eta$ )	Mean ( $\mu$ )	Var. ( $\sigma^2$ )	Skew. ( $\eta$ )
40848	-7.39	4.73	2.84	0.10	-0.84	2.65	2.66	0.12	-0.89	8.37	-0.92	1.31	5.18	-0.09
99566	-15.36	9.54	4.61	0.10	-0.09	6.26	-1.07	0.09	-2.98	33.31	-0.98	-1.53	39.01	0.00
40818	1.19	2.35	-0.98	0.07	1.02	3.79	-2.22	0.11	0.45	3.45	0.20	-0.05	9.70	0.14
99646	-9.59	6.77	4.73	0.09	-2.53	9.32	5.89	0.06	-0.64	16.99	-0.95	-1.03	39.05	-0.58
40847	-38.56	5.62	3.17	0.09	4.79	7.94	-4.90	0.08	-1.31	11.48	-0.99	1.30	24.59	0.84
40844	-29.80	7.92	4.02	0.10	10.63	1.51	-0.77	0.17	-2.30	22.83	-0.99	0.43	0.84	0.96
99580	-8.69	8.15	4.91	0.08	4.47	12.18	-8.02	0.08	-1.55	24.72	-0.94	1.47	58.37	0.82
88190	-3.63	4.98	3.73	0.08	-1.28	5.98	5.55	0.05	-0.10	10.14	-0.75	1.79	21.57	-0.23
40861	-7.31	7.08	4.55	0.09	4.04	8.51	-4.80	0.08	-1.05	18.80	-0.92	1.79	28.98	0.79
99561	-6.14	3.92	2.67	0.09	2.28	5.89	-3.62	0.08	-0.42	5.84	-0.90	0.68	16.14	0.53
40828	-0.58	4.04	0.86	0.10	1.47	6.35	-4.06	0.08	-0.75	13.76	-0.04	0.12	22.80	0.29
40855	-5.10	4.33	2.92	0.07	-0.64	5.05	2.15	0.09	-0.48	7.27	-0.86	-0.02	20.75	-0.05
40869	-12.17	4.18	2.84	0.09	-1.50	5.37	2.89	0.08	-0.48	6.43	-0.97	-0.67	16.15	-0.30
40862	-7.37	4.34	2.87	0.10	-4.04	6.06	3.76	0.10	-0.55	7.05	-0.92	-0.94	14.72	-0.79
99607	-35.62	4.65	2.80	0.09	-1.64	4.75	2.24	0.09	-0.91	7.86	-0.99	-1.00	12.08	-0.35
40859	-3.13	5.43	3.42	0.09	-2.02	7.40	4.42	0.07	-0.71	12.48	-0.69	-0.88	26.81	-0.46
40873	-3.63	5.49	4.16	0.08	-2.23	7.55	4.70	0.07	-0.06	12.31	-0.75	-0.80	26.84	-0.51
99575	-3.43	5.65	3.07	0.09	-2.28	8.18	5.43	0.10	-1.26	13.20	-0.73	-0.54	31.19	-0.53
99516	-2.36	3.21	2.46	0.07	3.59	5.89	-4.13	0.08	0.10	4.75	-0.55	0.39	14.18	0.74
99579	3.55	5.14	-3.94	0.13	1.31	5.10	-3.29	0.08	0.01	10.83	0.74	-0.06	15.55	0.24
99590	-1.22	4.54	3.18	0.09	-3.33	6.75	3.90	0.08	0.37	12.80	-0.21	-1.25	18.93	-0.71
99630	-5.69	6.14	3.95	0.10	-1.93	6.65	4.81	0.08	-0.87	14.42	-0.88	0.09	22.00	-0.44
40864	-2.64	5.41	4.07	0.08	1.99	7.49	-4.10	0.07	0.04	12.96	-0.60	1.24	27.58	0.45



**Fig. 7** Reliability evaluation of PERSIANN and TRMM daily rainfall data as a function of acceptable error domain

where erf() is error function<sup>5</sup> and  $T()$  is Owen’s  $T$  function<sup>6</sup>. The equation substantially indicates the cumulative probability of absolute value of the error to be less than  $E$ . Figure 7 compares reliability variation of PERSIANN and TRMM with acceptable error range in the stations of study area. At the beginning of the graph, in lower threshold levels of acceptable error, a sharp increase in the reliability is

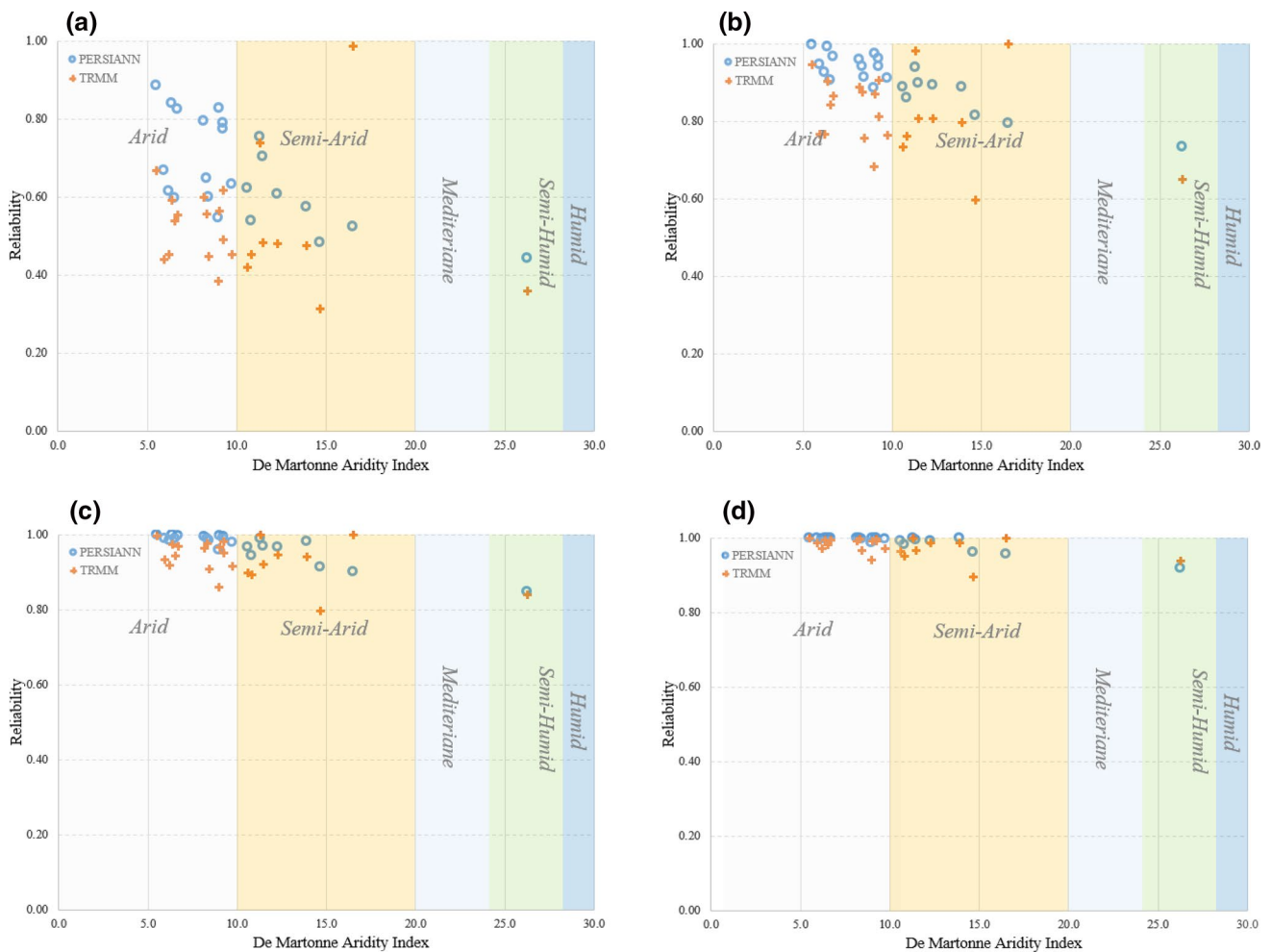
<sup>5</sup>  $\text{erf}(x) = \frac{2}{\sqrt{\pi}} \int_0^x e^{-t^2} dt.$

<sup>6</sup>  $T(x, a) = \frac{1}{2\pi} \int_0^a \frac{e^{-\frac{1}{2}x^2(1+t^2)}}{1+t^2} dt.$

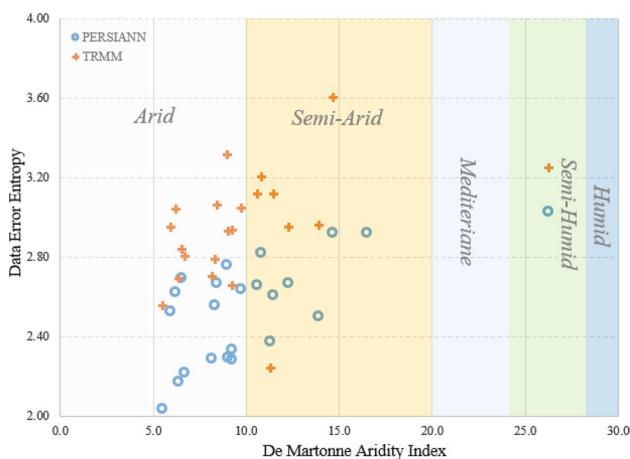
observed for both satellites. The rise is followed by attenuated growth for the broadening acceptable error ranges. In addition to overall behavior of the curves, the graphs that represent TRMM seem to be more widely scattered than the PERSIANN. Since the compacted curves indicate more chance to develop some trends for the error variation of the data, the PERSIANN satellite daily rainfall data are more consistent than the daily data obtained from TRMM satellite.

Figure 8 illustrates behavior of PERSIANN and TRMM SDDPD and clarifies their possible climatological consistency. Regarding the figures, a harmonious relation can be visually found between reliability of PERSIANN daily rainfall data and the climatological indicator in low ( $E = 3 \text{ mm/day}$ ) and medium ( $E = 6 \text{ mm/day}$ ) threshold levels, while no remarkable correlation exists between the data related to TRMM satellite and De Martonne aridity Index in the aforementioned domains. However, a near complete reliability can be found in higher threshold levels ( $E \geq 9 \text{ mm/day}$ ) for both satellite-derived precipitation data sets.

Figure 9 depicts the uncertainty of PERSIANN and TRMM data errors in terms of the Shannon entropy in coordination with the stations in the study area. It can be clearly observed that the parameter for the satellites differs in such way that one can claim that the PERSIANN satellite daily rainfall errors have lower uncertainty in several climatological situations in the study area. In addition, for both of the satellites, the daily rainfall errors uncertainty gradually increases with growth of De Martonne aridity Index, which



**Fig. 8** Reliability to PERSIANN and TRMM daily rainfall data with acceptance errors: **a**  $E = \pm 3$  mm/day, **b**  $E = \pm 6$  mm/day, **c**  $E = \pm 9$  mm/day, and **d**  $E = \pm 12$  mm/day



**Fig. 9** Entropy of PERSIANN and TRMM simulated daily rainfall error distribution

means that daily rainfall errors for both satellites are more certain in the arid climate.

Relative entropy, which is defined as the ratio of data error entropy to its highest possible value and being calculated as in Eq. 14, can be used to remove the scale parameter from data error. This quantity is a good measure to determine and compare the uncertainty of data error in various data domain sections. Recognition of domains with more error uncertainty helps to develop a clear vision of error resources and more efficient strategies to rectify them.

$$H_r(\text{ERR}) = \frac{H(\text{ERR})}{H_{\max}(\text{ERR})} = \begin{cases} \frac{H(E)}{\ln N}, & \text{empirical data set} \\ 1 - \frac{\psi}{H_{ND}}, & \text{the modeled pdf} \end{cases} \quad (14)$$

The more uniformity of the data error distribution along the data domain, the closer the relative entropy is to unity. Since homogeneous data error made error detection more difficult, the lower relative entropy of the data error is more

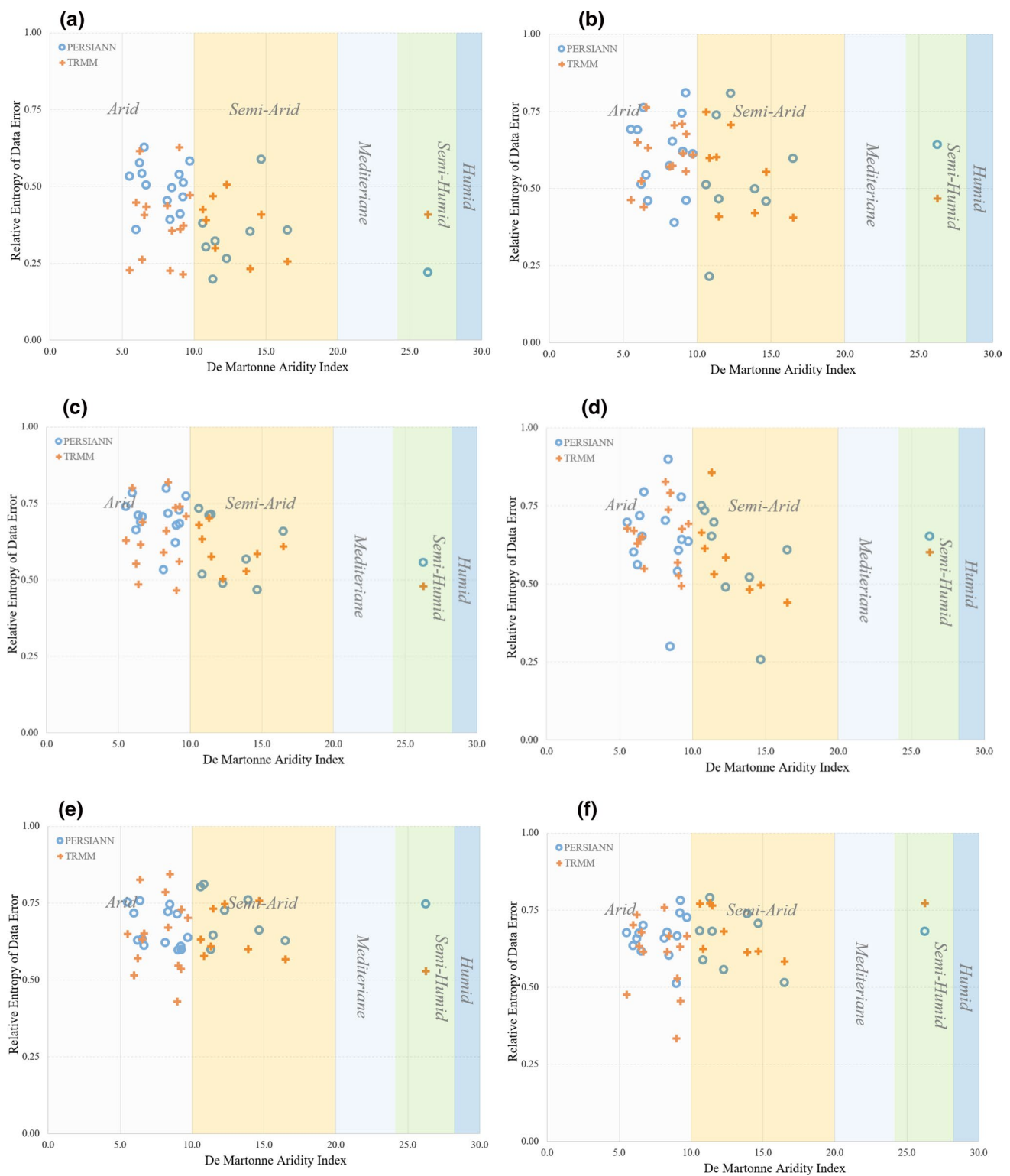
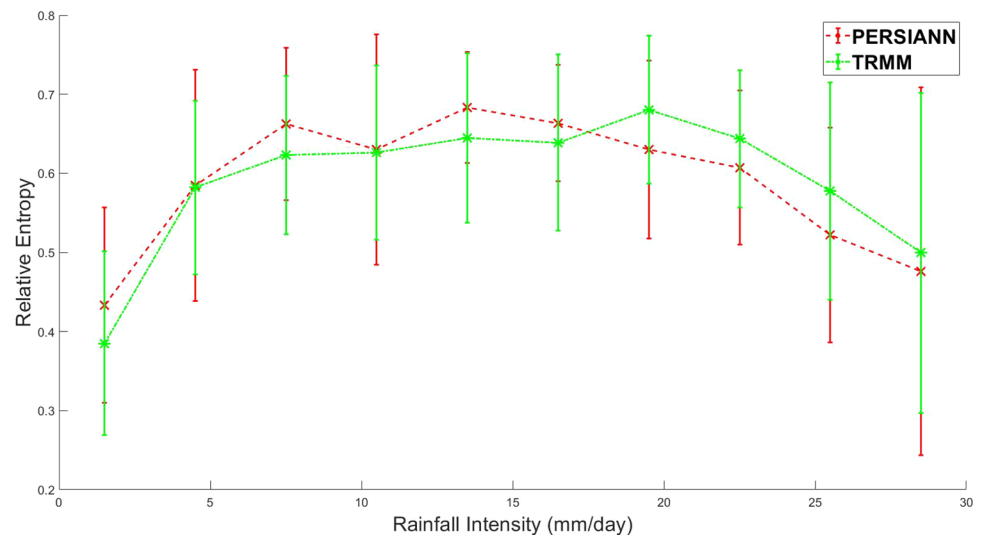


**Fig. 10** Relative Entropy of PERSIANN and TRMM daily rainfall error for: **a** daily rainfall less than 3 mm, **b** daily rainfall between 3 and 6 mm, **c** daily rainfall between 6 and 9 mm, **d** daily rainfall

between 9 and 12 mm, **e** daily rainfall between 12 and 15 mm, and **f** daily rainfall between 15 and 18 mm



**Fig. 11** PERSIANN and TRMM daily rainfall data error relative entropy for various rainfall intensities in the study area



favorable. For example, a data set with lower data error relative entropy seems to have error concentration about a certain value. If the value can be ignored, as the simplest way for error deletion, the accuracy of the data increases enormously. Therefore, lower values for data error entropy are desirable.

Figures 10 and 11 show variation of daily rainfall data error relative entropy with respect to daily rainfall intensity for PERSIANN and TRMM satellites. Figure 10 implies invariance of the parameter as an uncertainty index, in both climatological conditions, i.e., arid and semiarid climates, for almost all rainfall intensities. However, Fig. 11 shows a slight discrepancy in the relative entropies between PERSIANN and TRMM satellites daily rainfall data error, and it is possible to infer that the uncertainty of TRMM satellite daily rainfall data error for lower daily rainfall intensities is less than similar data uncertainty of PERSIANN satellite. On the contrary, the error uncertainty index of TRMM satellite daily rainfall error is quite higher in rather heavily rainy days in the study area.

As a summary of the discussion, reliable, certain and valid precipitation data are key requirements of plenty of hydrological models. However, high expenses and inaccessibility to precise ground-based observations to obtain the most reliable, certain and valid precipitation data affects the performance of such models. Therefore, in recent decades, the utilization of remote sensed precipitation data in water management, hydrological simulations and other water-related activities, besides strategic necessities to evaluate them considerably increased.

The present study has tried to address some shortcomings of previous studies. In Salmani-Dehaghi and Samani (2019), as a research in which the study area is exactly the same as the present study, it is concluded that PERSIANN, in all spatiotemporal scales, reflects the ground-based precipitation

observation pattern, but underestimate the precipitation in the study area. The finding of this paper has direct correspondence with the results in the aforementioned study. However, in addition to comparing the pattern of rainfall data calculated by algorithms based on satellite data and ground-based observations, this study analyzes the error values of satellite data in terms of reliability and certainty degree. It is concluded that satellite-derived precipitation products have higher reliability and certainty degree in arid climate regions of the study area. Furthermore, the results of other studies that cover the study area and satellites used in this research (e.g., Darand et al. 2017; Javanmard et al. 2010; Moazami et al. 2013, 2016) have more or less acceptable agreement with the results of this study in terms of accuracy, but firstly, the effect of climate on the results has not been investigated, and in addition, the reliability and uncertainty degree of the satellite-based precipitation data and their error have not been thoroughly explained. So, it is difficult to employ such data in hydrological or environmental simulations, for instance, flood warning models (Nguyen et al. 2015), in which nature of uncertainty of input data should be quantitatively explored.

This research also moves toward two specific goals. Firstly, it was tried to use the underlying concepts of reliability, uncertainty/certainty and validity, as identified statistical approaches, to assess satellite-derived daily precipitation data over the study area separately, and secondly, probable links between their quality and the climate conditions were checked. The principal findings are summarized as follows:

1. Among common cross-validating attributes, Pearson and Spearman rank correlation coefficients do not reflect useful outputs to validate SDDPD, nor can they be used to examine the effect of regional climates on the quality of this data. However, the values of ME and BIAS,

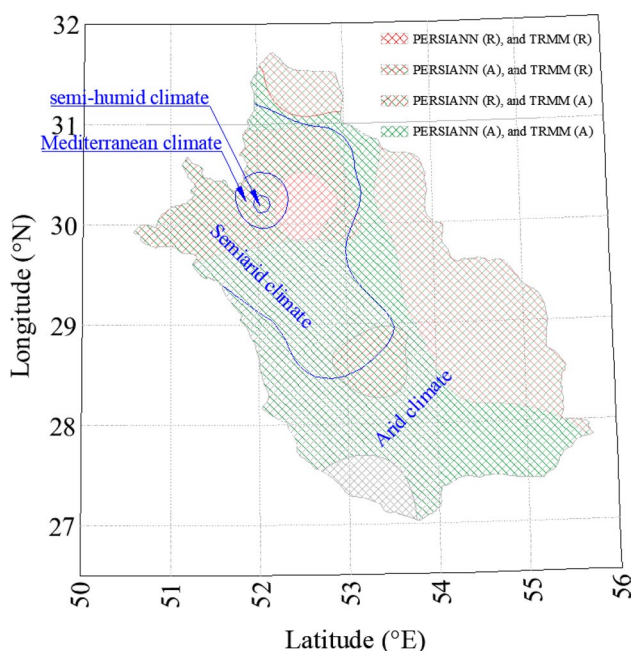


**Fig. 12** Regional classification of the study area according to Kolmogorov–Smirnov statistic in Accepting (A) or Rejecting (R) the hypothesis for harmonic behavior of satellite-based (PERSIANN and TRMM) daily precipitation with ground-based observations

in addition to RMSE and MAE, lead to the conclusion that PERSIANN almost underestimates the rainfall daily rates while TRMM overestimates the values mainly in semiarid regions. Besides, the PERSIANN is found to be significantly correlated with IDM, and the value of underestimation increases with growth of the index.

2. Making an appropriate analogy between cdfs of SDDPD and rain gauge observations indicates that TRMM and PERSIANN follow quite similar probability pattern of rain gauge observations in arid and semiarid climate, respectively. However, the pattern of the probability distribution function for the data for TRMM cannot be considered similar to rain gauge observations in arid region, just as PERSIANN in semiarid climate cannot. For more details, Fig. 12 shows quality of SDDPD over the study area with regard to data pattern analogy. According to the map, except in the eastern and southeastern regions of the study area, TRMM follows similar probability pattern of rain gauge observations. In addition, removing northwestern corner and a central spot, PERSIANN follows similar probability pattern of rain gauge observation.
3. The reliability values of SDDPD over the study area, for both TRMM and PERSIANN, have a reverse trend with increasing IDM values at almost all acceptable intervals. In other words, in terms of statistical reliability,

SDDPD in arid climate are more expected to be correctly detecting the rain gauge observations with presumed threshold. In addition to effects of climate conditions, the reliability indices of PERSIANN seem quite more consistent with different thresholds in comparison with the corresponding values of TRMM.

4. The SDDPD error entropy, as an index for uncertainty degree, increases as IDM rises, which is theoretically corresponding with reliability concept. However, in comparison with PERSIANN, TRMM, in overall, has higher degree of uncertainty. In addition, to evaluate effect of daily rainfall intensity on the uncertainty degree of SDDPD, the uncertainty degree slightly increased as daily rainfall intensified to about 15 mm/day. But for higher daily rainfall intensities, on the other hand, the uncertainty degree seems to gradually decline as the daily rainfall increases.

In brief, the concluding remarks are summarized in Table 6.

## Conclusions

In this study, two widely used precipitation products (TRMM 3B42RT and PERSIANN) were evaluated against rain gauge data over prevailing climates (arid and semiarid) in Fars province located in southwest of Iran during nearly a twenty-year period. The evaluation shows that “probability distribution pattern” of TRMM is in agreement with ground-based observations in the semiarid climate just as the PERSIANN in the arid climate. The Kolmogorov–Smirnov index, on the other hand, rejects the conformity of the probability distribution pattern of the ground-based observation to TRMM data in arid climates and to PERSIANN data in semiarid climates. Among common cross-validating attributes, the values of ME and BIAS, in addition to RMSE and MAE, lead to the conclusion that in the PERSIANN almost underestimates the rainfall daily rates while TRMM overestimates the values mainly in semiarid regions. Besides, the PERSIANN is found to be significantly correlated with IDM, and the values of underestimation increase with growth of the index. The reliability degree of SDDPD over the study area, for both TRMM and PERSIANN, decreases as the IDM increases for almost all acceptable error thresholds. Along with effects of climate conditions, the reliability indices of PERSIANN seem quite more consistent with different acceptable error thresholds in comparison with the corresponding values of TRMM. The entropy of SDDPD error, as an index for uncertainty degree, increases as IDM rises, which is theoretically corresponds with reliability concept. However, in comparison with PERSIANN, TRMM, in overall, have higher degree of uncertainty. In addition, to evaluate effect of daily rainfall intensity on the uncertainty degree

**Table 6** Performance characterization of PERSIANN and TRMM in terms of validations, reliability and certainty indices

	Arid climate		Semiarid climate		Semi-humid climate	
	PERSIANN	TRMM	PERSIANN	TRMM	PERSIANN	TRMM
<i>Validity indices</i>						
Comparing the cdfs of SDDPD and rain gauge observations	Almost accepted	Almost rejected	Almost rejected	Almost accepted	–	–
Pearson coefficient of correlation	No clear conclusion can be drawn					
Spearman coefficient of rank correlation	No clear conclusion can be drawn					
Root-mean-square error (RMSE)	Gradually increasing with growth of IDM	No clear conclusion can be drawn	Gradually increasing with growth of IDM	No clear conclusion can be drawn	–	–
Mean Error (ME)	Underestimates and decreasing with growth of IDM	No clear conclusion can be drawn	Underestimates and decreasing with growth of IDM	Overestimates, but no correlation with climate conditions	Underestimates	–
Mean Absolute Error (MAE)	Increasing with growth of IDM	No correlation with climate conditions	Increasing with growth of IDM	No correlation with climate conditions	–	–
Relative Bias (BIAS)	Underestimates and decreasing with growth of IDM	No clear conclusion can be drawn	Underestimates and decreasing with growth of IDM	Overestimates, but no correlation with climate conditions	Underestimates	–
<i>Reliability index</i>	Decreasing as the IDM increases	Decreasing as the IDM increases	Decreasing as the IDM increases	Decreasing as the IDM increases	–	–
<i>Certainty degree index</i>	The reliability indices of PERSIANN are more consistent in comparison with the corresponding values of TRMM		Decreasing as the IDM increases	Decreasing as the IDM increases	–	–
	Decreasing as the IDM increases		The certainty degree of the PERSIANN is higher than the value for TRMM		–	–
	Slightly increases as daily rainfall intensified to about 15 mm/day, but for higher daily rainfall intensities, the uncertainty degree gradually declines as the daily rainfall increase				–	–

of SDDPD, the uncertainty degree slightly increases as daily rainfall intensified to about 15 mm/day. But for higher daily rainfall intensities, on the other hand, the uncertainty degree seems to gradually decline as the daily rainfall increases.

This article tries to take a new look at the analysis of the reliability and certainty of satellite-derived precipitation data at a medium temporal resolution, i.e., daily. By the way, the need for more stations does not seem reasonable with regard to uniformity in results reflected by current stations. However, it is suggested that other researchers use the proposed procedures to analyze reliability and certainty degree of satellite-derived precipitation data for other temporal scales, regions and climate conditions, beside huge number of studies on indicators of validation.

### Appendix: Entropy of skew-normal distribution

The skew-normal distribution is an extension of the normal (Gaussian) probability distribution, allowing for the presence of skewness. This model and its variants have attracted the attention of an increasing number of research. The probability density function (pdf) of the skew-normal distribution with parameter  $\alpha$  is given by:

$$f(x) = 2\phi\left(\frac{x - \xi}{w}\right)\Phi\left(\alpha, \frac{x - \xi}{w}\right),$$

where

$$\begin{cases} \phi(t) = \frac{1}{w\sqrt{2\pi}}e^{-t^2} \\ \Phi(t, \alpha) = \frac{1}{2}[1 + \text{erf}(\alpha t)] \end{cases} \quad t = \frac{x - \xi}{w\sqrt{2}}$$

in which  $\phi(t)$  represents the normally distributed part and  $\Phi(t)$  tilted it to characterize the skewness.

Establishing some algebraic procedure to determine the entropy of the skew-normal distribution, it can be calculated as:

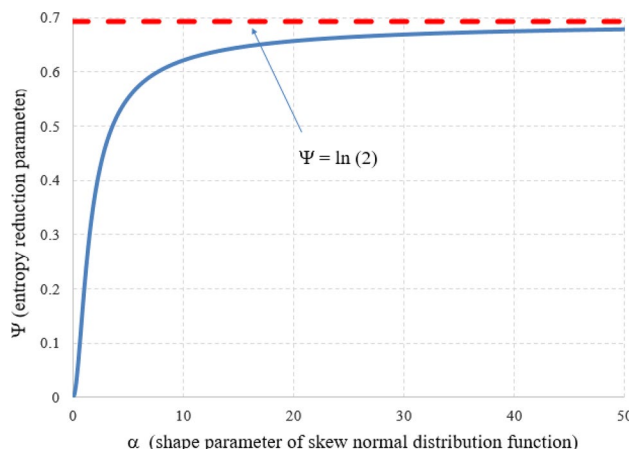
$$H_{SN} = H_N - E(\ln(2\Phi(x, \alpha))),$$

where  $H_N$  is entropy of normally distributed function ( $H_N = \frac{1}{2} + \frac{1}{2}\ln(2\pi w^2)$ ). The following procedure shows that expectation of  $\ln(2\Phi(x, \alpha))$  is just related to skewness factor  $\alpha$ .

$$\Psi(\alpha) = E(\ln(2\Phi(x, \alpha))) = \int_{-\infty}^{+\infty} 2\phi(x)\Phi(\alpha, x) \ln(2\Phi(\alpha, x))dx \Rightarrow$$

$$\Psi(\alpha) = \frac{1}{\sqrt{\pi}} \int_{-\infty}^{+\infty} e^{-t^2} [1 + \text{erf}(\alpha t)] \ln [1 + \text{erf}(\alpha t)] dt .$$

The value is defined as “entropy reduction parameter” and can be identified from the following diagram:



### Declarations

**Conflict of interest** On behalf of all authors, the corresponding author states that there is no conflict of interest.

### References

Adeyewa ZD, Nakamura K (2003) Validation of TRMM radar rainfall data over major climatic regions in Africa. *J Appl Meteorol* 42(2):331–347

AghaKouchak A, Mehran A, Norouzi H, Behrangi A (2012) Systematic and random error components in satellite precipitation data sets. *Geophys Res Lett* 39(9)

Amorocho J, Espildora B (1973) Entropy in the assessment of uncertainty in hydrologic systems and models. *Water Resour Res* 9(6):1511–1522

Arellano-Valle RB, Contreras-Reyes JE, Genton MG (2013) Shannon entropy and mutual information for multivariate skew-elliptical distributions. *Scand J Stat* 40(1):42–62

Awange JL, Ferreira VG, Forootan E, Khandu, Andam-Akorful SA, Forootan E, Agutu NO, He XF (2016) Uncertainties in remotely sensed precipitation data over Africa. *Int J Climatol* 36(1):303–323

Baltas E (2007) Spatial distribution of climatic indices in northern Greece. *Meteorol Appl* 14(1):69–78

Birolini A (2017) Basic concepts, quality & reliability (RAMS) assurance of complex equipment & systems, reliability engineering: theory and practice. Springer, Berlin, pp 1–24

Bitjukov SI, Maksimushkina AV, Smirnova VV (2016) Comparison of histograms in physical research. *Nucl Energy Technol* 2(2):108–113

Caloiero T, Veltri S, Caloiero P, Frustaci F (2018) Drought analysis in Europe and in the Mediterranean Basin using the standardized precipitation index. *Water* 10(8):1043

Camici S, Ciabatta L, Massari C, Brocca L (2018) How reliable are satellite precipitation estimates for driving hydrological models: a verification study over the Mediterranean area. *J Hydrol* 563:950–961

- Chen S, Hong Y, Cao Q, Gourley JJ, Kirstetter P-E, Yong B, Tian Y, Zhang Z, Shen Y, Hu J, Hardy J (2013a) Similarity and difference of the two successive V6 and V7 TRMM multisatellite precipitation analysis performance over China. *J Geophys Res Atmos* 118(23):13060–13074
- Chen S, Hong Y, Gourley JJ, Huffman GJ, Tian Y, Cao Q, Yong B, Kirstetter P-E, Hu J, Hardy J, Li Z, Khan SI, Xue X (2013b) Evaluation of the successive V6 and V7 TRMM multisatellite precipitation analysis over the Continental United States. *Water Resour Res* 49(12):8174–8186
- Darand M, Amanollahi J, Zandkarimi S (2017) Evaluation of the performance of TRMM multi-satellite precipitation analysis (TMPA) estimation over Iran. *Atmos Res* 190:121–127
- De Martonne E (1926) Une nouvelle fonction climatologique: L'indice d'aridité. *La Meteorologie* 2:449–458
- Derin Y, Yilmaz KK (2014) Evaluation of multiple satellite-based precipitation products over complex topography. *J Hydrometeorol* 15(4):1498–1516
- Dinku T, Chidzambwa S, Ceccato P, Connor SJ, Ropelewski CF (2008) Validation of high-resolution satellite rainfall products over complex terrain. *Int J Remote Sens* 29(14):4097–4110
- Dinku T, Ceccato P, Connor SJ (2011) Challenges of satellite rainfall estimation over mountainous and arid parts of east Africa. *Int J Remote Sens* 32(21):5965–5979
- Duan Z, Bastiaanssen WGM, Liu J (2012) Monthly and annual validation of TRMM multisatellite precipitation analysis (TMPA) products in the Caspian Sea Region for the period 1999–2003. Paper presented at the 2012 IEEE international geoscience and remote sensing symposium
- Ebert EE (2007) Methods for verifying satellite precipitation estimates. In: Levizzani V, Bauer P, Turk FJ (eds) *Measuring precipitation from space: EURAINSAT and the future*. Springer, Dordrecht, pp 345–356
- Emadodin I, Reinsch T, Taube F (2019) Drought and Desertification in Iran. *Hydrology* 6(3):66
- Gadgil S, Narayana Iyengar R (1980) Cluster analysis of rainfall stations of the Indian peninsula. *Q J R Meteorol Soc* 106(450):873–886
- Gao X, Zhu Q, Yang Z, Wang H (2018) Evaluation and hydrological application of CMADS against TRMM 3B42V7, PERSIANN-CDR, NCEP-CFSR, and gauge-based datasets in Xiang River Basin of China. *Water* 10(9):1225
- Geng Q, Wu P, Zhao X, Wang Y (2014) Comparison of classification methods for the divisions of wet/dry climate regions in Northwest China. *Int J Climatol* 34(7):2163–2174
- Gilewski P (2021) Impact of the grid resolution and deterministic interpolation of precipitation on rainfall-runoff modeling in a sparsely gauged mountainous catchment. *Water* 13(2):230
- Gilewski P, Nawalany M (2018) Inter-comparison of rain-gauge, radar, and satellite (IMERG GPM) precipitation estimates performance for rainfall-runoff modeling in a mountainous catchment in Poland. *Water* 10(11):1665
- Gourley JJ, Hong Y, Flamig ZL, Li L, Wang J (2010) Intercomparison of rainfall estimates from radar, satellite, gauge, and combinations for a season of record rainfall. *J Appl Meteorol Climatol* 49(3):437–452
- Gumindoga W, Rientjes THM, Haile AT, Makurira H, Reggiani P (2019) Performance evaluation of CMORPH satellite precipitation product in the Zambezi Basin. *Int J Remote Sens* 40(20):7730–7749
- Gupta HV, Wagener T, Liu Y (2008) Reconciling theory with observations: elements of a diagnostic approach to model evaluation. *Hydrol Process* 22(18):3802–3813
- Gupta HV, Kling H, Yilmaz KK, Martinez GF (2009) Decomposition of the mean squared error and NSE performance criteria: implications for improving hydrological modelling. *J Hydrol* 377(1):80–91
- Heydarizad M, Raeisi E, Sori R, Gimeno L, Nieto R (2018) The role of moisture sources and climatic teleconnections in Northeastern and South-Central Iran's hydro-climatology. *Water* 10(11):1550
- Heydarizad M, Raeisi E, Sori R, Gimeno L (2019) Developing meteoric water lines for Iran based on air masses and moisture sources. *Water* 11(11):2359
- Hirpa FA, Gebremichael M, Hopson T (2010) Evaluation of high-resolution satellite precipitation products over very complex terrain in Ethiopia. *J Appl Meteorol Climatol* 49(5):1044–1051
- Islam MA, Yu B, Cartwright N (2020) Assessment and comparison of five satellite precipitation products in Australia. *J Hydrol* 590:125474
- Javanmard S, Yatagai A, Nodzu MI, BodaghJamali J, Kawamoto H (2010) Comparing high-resolution gridded precipitation data with satellite rainfall estimates of TRMM\_3B42 over Iran. *Adv Geosci* 25:119–125
- Kidd C, Levizzani V (2011) Status of satellite precipitation retrievals. *Hydrol Earth Syst Sci* 15(4):1109–1116
- Kidd C, Bauer P, Turk J, Huffman GJ, Joyce R, Hsu KL, Braithwaite D (2012) Intercomparison of high-resolution precipitation products over northwest Europe. *J Hydrometeorol* 13(1):67–83
- Krakauer NY, Pradhanang SM, Lakhankar T, Jha AK (2013) Evaluating satellite products for precipitation estimation in mountain regions: a case study for Nepal. *Remote Sens* 5(8):4107–4123
- Langat PK, Kumar L, Koech R (2019) Identification of the most suitable probability distribution models for maximum, minimum, and mean streamflow. *Water* 11(4):734
- Li C, Tang G, Hong Y (2018) Cross-evaluation of ground-based, multi-satellite and reanalysis precipitation products: applicability of the triple collocation method across Mainland China. *J Hydrol* 562:71–83
- Liu J, Duan Z, Jiang J, Zhu AX (2015) Evaluation of three satellite precipitation products TRMM 3B42, CMORPH, and PERSIANN over a subtropical watershed in China. *Adv Meteorol* 2015:151239
- Liu S, Kang W, Wang T (2016) Drought variability in Inner Mongolia of northern China during 1960–2013 based on standardized precipitation evapotranspiration index. *Environ Earth Sci* 75(2):145
- Lu X, Tang G, Liu X, Wang X, Liu Y, Wei M (2021) The potential and uncertainty of triple collocation in assessing satellite precipitation products in Central Asia. *Atmos Res* 252:105452
- Martinez-Villalobos C, Neelin JD (2019) Why do precipitation intensities tend to follow gamma distributions? *J Atmos Sci* 76(11):3611–3631
- Masood M, Shakir AS, Azhar AH, Nabi G, Habib u, R. (2020) Assessment of real time, multi-satellite precipitation products under diverse climatic and topographic conditions. *Asia-Pac J Atmos Sci* 56(4):577–591
- Melo DCD, Xavier AC, Bianchi T, Oliveira PTS, Scanlon BR, Lucas MC, Wendland E (2015) Performance evaluation of rainfall estimates by TRMM multi-satellite precipitation analysis 3B42V6 and V7 over Brazil. *J Geophys Res Atmos* 120(18):9426–9436
- Michaelides S, Levizzani V, Anagnostou E, Bauer P, Kasparis T, Lane JE (2009) Precipitation: measurement, remote sensing, climatology and modeling. *Atmos Res* 94(4):512–533
- Moazami S, Golian S, Kavianpour MR, Hong Y (2013) Comparison of PERSIANN and V7 TRMM multi-satellite precipitation analysis (TMPA) products with rain gauge data over Iran. *Int J Remote Sens* 34(22):8156–8171
- Moazami S, Golian S, Hong Y, Sheng C, Kavianpour MR (2016) Comprehensive evaluation of four high-resolution satellite precipitation products under diverse climate conditions in Iran. *Hydrol Sci J* 61(2):420–440

- Mosaffa H, Shirvani A, Khalili D, Nguyen P, Sorooshian S (2020) Post and near real-time satellite precipitation products skill over Karkheh River Basin in Iran. *Int J Remote Sens* 41(17):6484–6502
- Nair S, Srinivasan G, Nemani R (2009) Evaluation of multi-satellite TRMM derived rainfall estimates over a western state of India. *J Meteorol Soc Jpn Ser II* 87(6):927–939
- Nastos PT, Kapsomenakis J, Philandras KM (2016) Evaluation of the TRMM 3B43 gridded precipitation estimates over Greece. *Atmos Res* 169:497–514
- Nguyen P, Thorstensen A, Sorooshian S, Hsu K, AghaKouchak A (2015) Flood forecasting and inundation mapping using HiRes-Flood-UCI and near-real-time satellite precipitation data: the 2008 Iowa Flood. *J Hydrometeorol* 16(3):1171–1183
- Nicholson SE, Some B, McCollum J, Nelkin E, Klotter D, Berte Y, Diallo BM, Gaye I, Kpabeba G, Ndiaye O, Noukpozoukou JN, Tanu MM, Thiam A, Toure AA, Traore AK (2003a) Validation of TRMM and other rainfall estimates with a high-density gauge dataset for West Africa. Part I: validation of GPCC rainfall product and Pre-TRMM satellite and blended products. *J Appl Meteorol* 42(10):1337–1354
- Nicholson SE, Some B, McCollum J, Nelkin E, Klotter D, Berte Y, Diallo BM, Gaye I, Kpabeba G, Ndiaye O, Noukpozoukou JN, Tanu MM, Thiam A, Toure AA, Traore AK (2003b) Validation of TRMM and other rainfall estimates with a high-density gauge dataset for West Africa. Part II: validation of TRMM rainfall products. *J Appl Meteorol* 42(10):1355–1368
- Nourani V, Baghanam AH, Adamowski J, Gebremichael M (2013) Using self-organizing maps and wavelet transforms for space–time pre-processing of satellite precipitation and runoff data in neural network based rainfall–runoff modeling. *J Hydrol* 476:228–243
- Ochoa A, Pineda L, Crespo P, Willems P (2014) Evaluation of TRMM 3B42 precipitation estimates and WRF retrospective precipitation simulation over the Pacific-Andean region of Ecuador and Peru. *Hydrol Earth Syst Sci* 18(8):3179–3193
- O’Hagan A, Leonard TOM (1976) Bayes estimation subject to uncertainty about parameter constraints. *Biometrika* 63(1):201–203
- Paredes Trejo FJ, Alves Barbosa H, Peñaloza-Murillo MA, Moreno MA, Farías A (2016) Intercomparison of improved satellite rainfall estimation with CHIRPS gridded product and rain gauge data over Venezuela. *Atmósfera* 29:323–342
- Pellicone G, Caloiero T, Guagliardi I (2019) The De Martonne aridity index in Calabria (Southern Italy). *J Maps* 15(2):788–796
- Pipunic RC, Ryu D, Costelloe JF, Su C-H (2015) An evaluation and regional error modeling methodology for near-real-time satellite rainfall data over Australia. *J Geophys Res Atmos* 120(20):10767–10783
- Price K, Purucker ST, Kraemer SR, Babendreier JE, Knights CD (2014) Comparison of radar and gauge precipitation data in watershed models across varying spatial and temporal scales. *Hydrol Process* 28(9):3505–3520
- Prigent C (2010) Precipitation retrieval from space: an overview. *C R Geosci* 342(4):380–389
- Rahmawati N, Lubczynski MW (2018) Validation of satellite daily rainfall estimates in complex terrain of Bali Island, Indonesia. *Theor Appl Climatol* 134(1):513–532
- Robinson DW (2008) Entropy and uncertainty. *Entropy* 10(4):493–506
- Salmani-Dehaghi N, Samani N (2019) Spatiotemporal assessment of the PERSIANN family of satellite precipitation data over Fars Province, Iran. *Theor Appl Climatol* 138(3):1333–1357
- Sapiano MRP, Janowiak JE, Shi W, Higgins RW, Silva VBS (2010) Regional evaluation through independent precipitation measurements: USA. In: Gebremichael M, Hossain F (eds) *Satellite rainfall applications for surface hydrology*. Springer, Dordrecht, pp 169–191
- Scheel MLM, Rohrer M, Huggel C, Santos Villar D, Silvestre E, Huffman GJ (2011) Evaluation of TRMM multi-satellite precipitation analysis (TMPA) performance in the Central Andes region and its dependency on spatial and temporal resolution. *Hydrol Earth Syst Sci* 15(8):2649–2663
- Shaghaghian MR, Abedini MJ (2013) Rain gauge network design using coupled geostatistical and multivariate techniques. *Sci Iran* 20(2):259–269
- Sohn BJ, Han H-J, Seo E-K (2010) Validation of satellite-based high-resolution rainfall products over the Korean Peninsula using data from a dense rain gauge network. *J Appl Meteorol Climatol* 49(4):701–714
- Stamp LD, Wooldridge SW (1951) *London essays in geography: Rodwell Jones Memorial Volume*. Harvard University Press, Cambridge
- Su F, Hong Y, Lettenmaier DP (2008) Evaluation of TRMM multisatellite precipitation analysis (TMPA) and its utility in hydrologic prediction in the La Plata Basin. *J Hydrometeorol* 9(4):622–640
- Sun Q, Miao C, Duan Q, Ashouri H, Sorooshian S, Hsu K-L (2018) A review of global precipitation data sets: data sources, estimation, and intercomparisons. *Rev Geophys* 56(1):79–107
- Tabari H, Hosseinzadeh Talaei P, Mousavi Nadoushani SS, Willems P, Marchetto A (2014) A survey of temperature and precipitation based aridity indices in Iran. *Quat Int* 345:158–166
- Tan ML, Santo H (2018) Comparison of GPM IMERG, TMPA 3B42 and PERSIANN-CDR satellite precipitation products over Malaysia. *Atmos Res* 202:63–76
- Teegavarapu RSV (2019) Chapter 1—methods for analysis of trends and changes in hydroclimatological time-series. In: Teegavarapu R (ed) *Trends and changes in hydroclimatic variables*. Elsevier, Amsterdam, pp 1–89
- Thiemig V, Rojas R, Zambrano-Bigiarini M, Levizzani V, De Roo A (2012) Validation of satellite-based precipitation products over sparsely gauged African River Basins. *J Hydrometeorol* 13(6):1760–1783
- Thorntwaite C (1955) Mather, JR. *The water balance*. Drexel Institute of Technology–Laboratory of Climatology, Centerton, NJ, 104 p. *Publications in climatology*, vol 8(1)
- Tian Y, Peters-Lidard CD, Eylander JB, Joyce RJ, Huffman GJ, Adler RF, Hsu K, Turk FJ, Garcia M, Zeng J (2009) Component analysis of errors in satellite-based precipitation estimates. *J Geophys Res Atmos* 114(D24)
- Vallejo-Bernal SM, Urrea V, Bedoya-Soto JM, Posada D, Olarte A, Cárdenas-Posso Y, Ruiz-Murcia F, Martínez MT, Petersen WA, Huffman GJ, Poveda G (2021) Ground validation of TRMM 3B43 V7 precipitation estimates over Colombia. Part I: monthly and seasonal timescales. *Int J Climatol* 41(1):601–624
- Wilby RL, Wigley TML (2002) Future changes in the distribution of daily precipitation totals across North America. *Geophys Res Lett* 29(7):39-1-39-4
- Yang Y, Luo Y (2014) Evaluating the performance of remote sensing precipitation products CMORPH, PERSIANN, and TMPA, in the arid region of northwest China. *Theor Appl Climatol* 118(3):429–445
- Yong B, Ren L-L, Hong Y, Wang J-H, Gourley JJ, Jiang S-H, Chen X, Wang W (2010) Hydrologic evaluation of multisatellite precipitation analysis standard precipitation products in basins beyond its inclined latitude band: a case study in Laohahe basin, China. *Water Resour Res* 46(7)
- Zambrano-Bigiarini M, Nauditt A, Birkel C, Verbist K, Ribbe L (2017) Temporal and spatial evaluation of satellite-based rainfall estimates across the complex topographical and climatic gradients of Chile. *Hydrol Earth Syst Sci* 21(2):1295–1320
- Zarghami M, Abdi A, Babaeian I, Hassanzadeh Y, Kanani R (2011) Impacts of climate change on runoffs in East Azerbaijan, Iran. *Glob Planet Change* 78(3):137–146

- Zhang Q, Sun P, Chen X, Jiang T (2011) Hydrological extremes in the Poyang Lake basin, China: changing properties, causes and impacts. *Hydrol Process* 25(20):3121–3130
- Zou KH, Tuncali K, Silverman SG (2003) Correlation and simple linear regression. *Radiology* 227(3):617–628
- Zubieta R, Getirana A, Espinoza JC, Lavado W (2015) Impacts of satellite-based precipitation datasets on rainfall–runoff modeling of the Western Amazon basin of Peru and Ecuador. *J Hydrol* 528:599–612
- Zulkafli Z, Buytaert W, Onof C, Manz B, Tarnavsky E, Lavado W, Guyot J-L (2014) A comparative performance analysis of TRMM 3B42 (TMPA) versions 6 and 7 for hydrological applications over Andean-Amazon River Basins. *J Hydrometeorol* 15(2):581–592